

Adiabatic Spectroscopy and a Variational Quantum Adiabatic Algorithm

Benjamin F. Schiffer,^{1, 2, *} Jordi Tura,^{3, 1, 2} and J. Ignacio Cirac^{1, 2}

¹*Max-Planck-Institut für Quantenoptik, Hans-Kopfermann-Str. 1, D-85748 Garching, Germany*

²*Munich Center for Quantum Science and Technology (MCQST), Schellingstr. 4, D-80799 Munich, Germany*

³*Instituut-Lorentz, Universiteit Leiden, P.O. Box 9506, 2300 RA Leiden, The Netherlands*

(Dated: December 23, 2024)

Preparing the ground state of a Hamiltonian is a problem of great significance in physics with deep implications in the field of combinatorial optimization. The adiabatic algorithm is known to return the ground state for sufficiently long preparation times which depend on the a priori unknown spectral gap. Our work relates in a twofold way. First, we propose a method to obtain information about the spectral profile of the adiabatic evolution. Second, we present the concept of a variational quantum adiabatic algorithm (VQAA) for optimized adiabatic paths. We aim at combining the strengths of the adiabatic and the variational approaches for fast and high-fidelity ground state preparation while keeping the number of measurements as low as possible. Our algorithms build upon ancilla protocols which we present that allow to directly evaluate the ground state overlap. We benchmark for a non-integrable spin-1/2 transverse and longitudinal Ising chain with $N = 53$ sites using tensor network techniques. Using a black box, gradient-based approach, we report a reduction in the total evolution time for a given desired ground state overlap by a factor of ten, which makes our method suitable for the limited decoherence time of noisy-intermediate scale quantum devices.

I. INTRODUCTION

Remarkable scientific progress in recent years has led to the first noisy intermediate-scale quantum (NISQ) [1] devices. Current NISQ devices are still limited by the number of qubits available, their gate fidelity and the maximum circuit depth. Much research effort is put into the investigation of algorithms for digital NISQ devices that could hold the promise of a (practical) quantum advantage [2, 3]. Nevertheless, simulating large quantum many-body systems on these devices still remains challenging within the next years. Analog quantum simulators, however, are able to implement some quantum dynamics very efficiently. Furthermore, analog quantum simulators are especially well suited for probing universal features of quantum many-body systems. Several powerful concepts and experimental realizations of digital NISQ devices and analog quantum simulators have been put forward [4–6].

One particularly important problem is preparing the ground state of quantum many-body systems, relevant for a wide range of physics applications and closely related to combinatorial optimization tasks. Quantum computers already save an exponential memory cost compared to a classical computer in the representation of the quantum state, making a quantum device the natural choice to compute desired quantum states. Moreover, ground states are also of great importance for optimization problems as the solutions to combinatorial problems can be naturally encoded into a classical Hamiltonian.

The ground state finding problem is known to be QMA-complete [7], which translates roughly to the analogue

of NP-complete for a quantum computer. However, two different promising heuristic approaches have been established. First and most straightforward, there is the adiabatic approach. In order to prepare the ground state of a target Hamiltonian H_T with a quantum adiabatic algorithm (QAA) [8], one takes an adiabatic path $H(s) = (1-s)H_0 + sH_T$. Starting from the ground state of a trivial Hamiltonian H_0 at $s(0) = 0$, the parameter $s(t)$ is changed with time until the final value $s(T) = 1$. Given a non-degenerate ground state along the path, the adiabatic algorithm is known to return the ground state for a sufficiently long preparation time T . However, T is a function of the spectral energy gap $\Delta(s)$ between the ground state and the first excited state along the adiabatic path and not known a priori [9–12]. Due to the limited decoherence times of current NISQ devices and analog quantum simulators, the preparation time T is of great relevance for the feasibility of the adiabatic approach. Different adiabatic paths can be constructed and a linear time schedule is generally not optimal in the sense of a minimal T . This is especially relevant when the gap $\Delta(s)$ becomes very small as it occurs in the presence of a quantum phase transition.

Another approach is the quantum approximate optimization algorithm (QAOA) [13] which seeks to overcome these limitations. It generalizes the QAA by splitting the total time into chunks, $\{T_i\}$, where one alternates between H_0 and H_T , and takes $\{T_i\}$ as the variational parameters. The QAOA includes the QAA in the sense that choosing $T_i = iT/L$, where $i = \{1, \dots, L\}$ and L sufficiently large, corresponds to the Trotter evolution of the QAA. However, it is expected that the QAOA can provide a speedup by choosing the parameters $\{T_i\}$ larger than in trotterized QAA.

In fact, the QAOA belongs to a wider class of variational quantum algorithms (VQA) in the spirit of the variational principle which is widely used in physics.

* Corresponding author: Benjamin.Schiffer@mpq.mpg.de

While the quantum computer is used to prepare the states and perform the measurements, the optimization of the parameters is carried out classically. In practice, the performance of VQA can be curbed since the number of measurements necessary to estimate an objective function may scale unfavorably, and due to the presence of plateaus in the energy landscape, including noise-induced barren plateaus [14–17].

In this work, we propose the concept of a variational quantum adiabatic algorithm (VQAA) to find optimal adiabatic paths for high-fidelity ground state preparation, thereby combining the strengths of adiabatic state preparation and VQA. Akin to the QAOA, the times $\{T_i\}$ are treated as the variational parameters. However, the evolution in the different chunks is performed adiabatically, similarly to the QAA. Here, the VQAA differs from the fixed Hamiltonians found in the QAOA. The VQAA allows for a significant acceleration compared to the QAA with a linear adiabatic path, yet requires fewer parameters and measurements than the QAOA.

We discuss different approaches to find such a parametrized optimal adiabatic path. The approaches are suited to different resource requirements, some making use of ancilla protocols to estimate the ground state overlap. These protocols rely on controlled unitary evolution which leads to many benefits in the quantum computing setting. Besides being central to the canonical quantum phase estimation algorithm [18], it also allows to access overlaps between initial and final states for a given unitary transformation by looking at the ancilla only and enables spectral projections on the state of the system if one enables postselection on the ancilla [19]. The ancilla techniques presented here may prove to be useful tools by themselves for other variational algorithms. We benchmark the different algorithms with a quantum Hamiltonian and up to $N = 100$ qubits, which is what is expected for the new generation of NISQ devices or analog quantum simulators. We take a Hamiltonian that is non-trivial (non-integrable) but for which we can simulate the action of a quantum computer classically using tensor network techniques. In the case of a small gap in the adiabatic path, in the presence of a phase transition, we report significant reductions in the required evolution time to reach a given desired ground state overlap. For a chain of $N = 53$ qubits and a target overlap of 90%, the VQAA is able to reduce the total evolution time by a factor of 10 compared to a linear adiabatic path.

Having mentioned before that the spectral gap $\Delta(s)$ is a priori unknown, obtaining knowledge about the spectral gap $\Delta(s)$ can be as hard a problem as finding the ground state itself. However, due to the interconnection between the spectral gap and the performance of adiabatic state preparation, we are able to propose a form of adiabatic spectroscopy to find spectral gap properties. Performing adiabatic sweeps on the system and being equipped with the ancilla protocols for ground state estimation,

a measure for both the position and the smallness of the spectral gap can be obtained. Knowledge about the spectral gap may be applied to gain important insights about quantum many-body physics, obtain the phase diagram of a physical system or formulate the optimal path for adiabatic state preparation.

The structure of this paper is as follows. In Section II we outline our main results. Then, we discuss our approach to adiabatic spectroscopy in Sec. III, and in Sec. IV, we present two protocols for estimating the ground state at a given point along the adiabatic path using one or two ancillas. In Sec. V, we introduce the general concept of a variational quantum adiabatic algorithm for ground state preparation and discuss different specific algorithms with different resource requirements (Sec. VI). After that, in Sec. VII, the model for benchmarking our algorithms is described and we present results. Finally, we comment on the number of measurements necessary in our approach (Sec. VIII) and the impact of noise on our algorithms (Sec. IX). In the Appendices, we give the necessary background to make the paper self-contained: a theoretical description of the adiabatic algorithm and QAOA as well as Bayesian inference for Beta-Bernoulli models which are relevant for performing hypothesis testing.

II. MAIN RESULTS

Our main results include (1) protocols for eigenstate closeness estimation, (2) a proposal for adiabatic spectroscopy, as well as a (3) concept for variational quantum adiabatic algorithms including a black box gradient-based method.

(1) Provided the possibility to implement controlled unitary evolution on a quantum state, where the dynamics are controlled by a single ancilla qubit, information about the closeness to the next eigenstate can be extracted from the ancilla. We show that for a quantum state $|\psi\rangle = \sum_j \psi_j |\phi_j\rangle$ and Hamiltonian $H = \sum_j E_j |\phi_j\rangle \langle \phi_j|$, we need to obtain $\alpha := \sum_j |\psi_j|^2 \exp(-iE_j \tau)$ by measuring the ancilla. Then, for suitable τ , we can deduce that the state $|\psi\rangle$ is an eigenstate of H only if $|\alpha| = 1$. By a self-consistent argument and suitable construction, the closest eigenstate may be identified with the ground state.

(2) The profile of the spectral gap $\Delta(s)$ between the ground state and first excited state energy of an interpolating Hamiltonian $H(s)$ is closely connected to the evolution time T required for adiabatic state preparation. We analyze the evolution time $T(s)$ necessary to prepare the ground state of $H(s)$ with a given target overlap. The ground state overlap is computed either by time-evolving both forward and backward and measuring the overlap with the initial product state, or by making use of the ancilla protocol which is generally expected to give superior results.

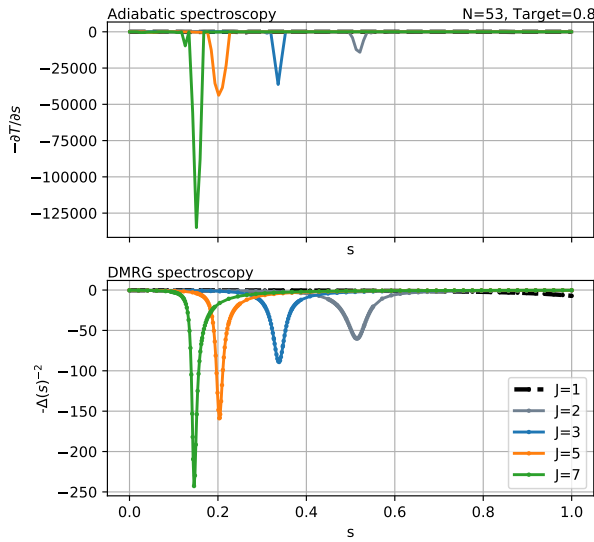


FIG. 1. Adiabatic spectroscopy for a chain of $N = 53$ qubits and a target ground state overlap of 0.7. For the Hamiltonian $H(J, g, h) = \sum_i (J\sigma_i^z\sigma_{i+1}^z + h\sigma_i^x + g\sigma_i^z)$, the adiabatic path is a linear interpolation from $H(0, 1, 0)$ to $H(J, 1, 1)$. The minima of the different curves correspond to position and smallness of the respective spectral gap. In the lower plot, $-\Delta(s)^{-2}$ is shown as a comparison, obtained with DMRG.

After obtaining the data points for $T(s)$, we interpolate the curve and compute the derivative. Corresponding to physical intuition, the curve of the evolution time features a strong increase when a small gap is crossed. The derivative $\partial T/\partial s$ can then provide the position and also a measure for the smallness of the spectral gap (Fig. 1).

(3) In our work, we present the concept of the VQAA and give specific algorithms which attempt to improve over QAA. The main idea is to optimize the adiabatic path $s(t)$ by performing a moderate number of measurements. In our setup, $s(t)$ depends on a set of parameters, which are chosen through optimization procedures. The key ingredient is to use the overlap with the ground state as the figure of merit. The algorithms presented in this work make use of different protocols to estimate this overlap, and are also distinguished in the way the optimization is performed: either by intending to remain in the ground state at intermediate steps in the adiabatic path, or by optimizing for a maximum ground state overlap at the end of the state preparation (like in QAOA). The main feature of the method presented in this paper is that it requires fewer measurements. Our approach is well suited to be used in NISQ devices or analog quantum simulators by reducing the required preparation time and thus avoiding decoherence. Without knowing the adiabatic spectrum beforehand, the optimal adiabatic paths yield the desired ground state with high fidelity at only a fraction of the total evolution time of a non-optimized adiabatic algorithm (Fig. 2).

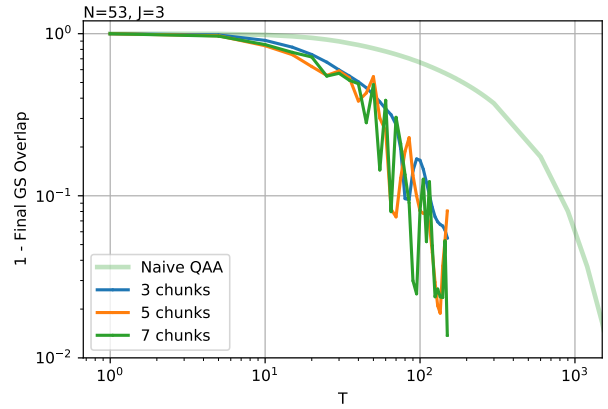


FIG. 2. Black box VQAA results for 53 qubits and the ZZXZ model for the case of a crossed phase transition ($J = 3$). Results for 3, 5 and 7 chunks, respectively, are shown. The quantum-classical feedback loop converges to optimized adiabatic paths that prepare the ground state with $> 90\%$ overlap for $T \lesssim 100$. In order to achieving this ground state overlap with (non-optimized) naive QAA would have required an evolution time about 10 times larger.

III. ADIABATIC SPECTROSCOPY

We seek to gain insights about the adiabatic spectrum of the Hamiltonian

$$H(s) = (1 - s)H_0 + sH_T. \quad (1)$$

The Hamiltonian $H(s)$ describes the adiabatic evolution from the ground state of a trivial Hamiltonian H_0 at $s = 0$ to the ground state of H_T at $s = 1$ where $s = t/T$ is parametrized time. The probability that the system transitions out of the ground state in the course of the evolution is intimately connected with the size of the spectral gap $\Delta(s) = E_1(s) - E_0(s)$ between the ground state and the first excited state energy. For each s_i in a set of data points $\{s_i\}$, $i \in \{1, \dots, r\}$ and r being the resolution of the spectroscopy, an efficient root finding algorithm is used (e.g. using a bisection algorithm on the time variable T_i) to find the evolution time T_i which reaches a given target ground state overlap O_T . If a small gap is crossed in the adiabatic path, e.g. at s^* , this will correspond to a large increase of the $\{T_i\}$ around and after this value s^* . Hence, if we observe such a rise in the required evolution times $\{T_i\}$, we conclude that a local minimum in the spectral gap $\Delta(s^*)$ must be present. In this manner, the position of a small spectral gap can be obtained. Moreover, the smallness of $\Delta(s^*)$ is related to the steepness of the increase in the $\{T_i\}$ around s^* . For the Landau-Zener model, we establish the relation $\partial T(s)/\partial s \sim 1/\Delta(s)^2$ around the minimal gap (App. B). Since the Landau-Zener approach is a toy model to qualitatively study the property of the spectral gap in adiabatic algorithms, we presume that a similar scaling could persist in a more general sense. In order to obtain a measure for the ground state overlap

for given s_i , we propose two different approaches. The first approach is not making use of the ancilla protocol and is thus very simple to implement. The initial ground state $|\psi_0\rangle$ at $s = 0$ is adiabatically time-evolved forward with evolution time \tilde{T}_j , implemented by the unitary operator $U_{0 \rightarrow s_i}(\tilde{T}_j)$. Here, the \tilde{T}_j denote the probing values in the search for the evolution time T_i which succeeds in reaching the given overlap O_T . Next, the interactions are reversed in a backward time evolution from $s = s_i$ to $s = 0$ implemented by $U_{0 \leftarrow s_i}(\tilde{T}_j)$. This allows for a trivial measurement of the ground state overlap at $s = 0$

$$\tilde{O}_j = \left| \langle \psi_0 | U_{0 \leftarrow s_i}(\tilde{T}_j) U_{0 \rightarrow s_i}(\tilde{T}_j) | \psi_0 \rangle \right| \quad (2)$$

as the state $|\psi_0\rangle$ is a product state. Once a \tilde{T}_j is found for which $\tilde{O}_j \approx O_T$, we set $T_i := \tilde{T}_j$ and proceed with the next data point s_{i+1} . Note that it is also sensible to use a large constant evolution time for the backwards path. We extend this approach by noting that if a small spectral gap $\Delta(s^*)$ has been found and we continue to probe for those s_i for which $s_i > s^*$, it is economical to make use of the spectral information already obtained. In the spirit of the VQAA, the adiabatic schedule used in the spectroscopy should be altered so that the evolution around s^* is performed very slowly. In this manner, multiple gaps in the adiabatic spectrum could be investigated. This ancilla-free approach provides the least stringent requirements on the experimental setup in a NISQ framework.

However, with some additional effort, there is the possibility with to directly estimate the ground state overlap without going back to the initial state at $s = 0$. This second approach leverages on the ability to obtain a measure for the eigenstate closeness through an ancilla protocol. For every data point in $\{s_i\}$, we obtain the ground state overlap for different \tilde{T}_j directly:

$$\tilde{O}'_j = \left| \langle \text{GS}_{s_i} | U_{0 \rightarrow s_i}(\tilde{T}_j) | \psi_0 \rangle \right|, \quad (3)$$

with $|\text{GS}_{s_i}\rangle$ the ground state at s_i . Now just like in the first approach, we search for the \tilde{T}_j such that $\tilde{O}'_j \approx O_T$ and set $T_i := \tilde{T}_j$.

Hence, this form of adiabatic spectroscopy can provide a tool in order to experimentally gain knowledge about the adiabatic spectrum. We simulate this technique classically with $N = 53$ qubits for different spectral profiles and present the results in (Fig. 1) and Sec. VII B.

IV. PROTOCOL FOR GROUND STATE CLOSENESS ESTIMATION

A very important ingredient of our algorithms is the ability to estimate the overlap with the ground state. In this section we introduce two suitable protocols using ancillas and comment briefly on their benefits. The

ancilla protocols only require the ability to implement unitary evolution controlled on a single ancilla and to perform measurements on the ancilla. Controlled unitary evolution is a valuable ingredient for quantum computing, e.g. in the well-known quantum phase estimation algorithm [18]. Using ancilla measurements for ground state preparation has been investigated previously and can be used to construct spectral projection operators similar to the quantum Zeno effect if one allows for postselection on the ancilla [19]. In our work, we utilize the ancilla in order to extract information about the eigenstate closeness which can then be used in the different applications of the VQAA in a highly versatile manner.

A. Single-ancilla protocol

We first present a protocol for eigenstate closeness estimation using a single ancilla in the $|+\rangle$ state [20]. The quantum circuit shown in (Fig. 3) can be used to compare the overlap of an initial quantum state $|\psi\rangle$ with

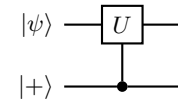


FIG. 3. Quantum circuit for unitary dynamics controlled by a single ancilla qubit in the $|+\rangle$ state.

the state after the unitary evolution $|\psi_{\text{evo}}\rangle$

$$\langle \psi | \psi_{\text{evo}} \rangle = \langle \sigma_x + i\sigma_y \rangle_{\text{ancilla}}. \quad (4)$$

For a fixed Hamiltonian $H = \sum_j E_j |\phi_j\rangle \langle \phi_j|$ with the unitary

$$U |\phi_j\rangle = e^{-iH\tau} |\phi_j\rangle = e^{-iE_j\tau} |\phi_j\rangle, \quad (5)$$

we write the normalized state $|\psi\rangle = \sum_j \psi_j |\phi_j\rangle$ in the eigenbasis of H . Then, we analyze the quantum circuit for this choice of U . We obtain for the density matrix of the ancilla qubit after the controlled unitary evolution (App. C 1)

$$\rho_a = \sum_j \frac{|\psi_j|^2}{2} \begin{pmatrix} 1 & e^{iE_j\tau} \\ e^{-iE_j\tau} & 1 \end{pmatrix}. \quad (6)$$

For a quantum state $|\psi\rangle$ that is an eigenstate, the rank of ρ_a will be 1. Due to the specific structure of ρ_a , only one off-diagonal matrix element is needed in order to determine the rank of ρ_a . We note with (Eqn. C4) that

$$\langle \psi | \psi_{\text{evo}} \rangle = \sum_j |\psi_j|^2 e^{-iE_j\tau} =: \alpha. \quad (7)$$

For suitable τ , $|\psi_{\text{evo}}\rangle$ is an eigenstate only if $|\alpha| = 1$. The time τ needs to be chosen so that the complex

summands of α with non-vanishing amplitude do not have approximately equal phases. In this unlikely case of matching phases, we would see constructive interference so that $|\alpha| = 1$ could be true even if $|\psi_{\text{evo}}\rangle$ is not an eigenstate. Visualizing the summands of α on a complex plane (Fig. 4), this becomes rather intuitive. The choice for τ is related to the spectrum of H . For the sake of this argument we assume that the overlap with the ground state and first excited state are the only other non-vanishing overlaps. Then, an arbitrary τ would correspond to choosing an $l \in \mathbb{Z}$ in $\tau = \pi l / \Delta$ at random (App. C3). For $l \gg 1$, the probability of choosing an odd value of l is approximately $1/2$. Therefore, by testing several random values of $\tau \in O(\Delta^{-1})$ it is possible to deduce information about the system whether it is in a mixed state or an eigenstate with high confidence (cf. the Chernoff-Hoeffding bound in Sec. VIII). Through a self-consistent argument we can conclude that the main contribution to α comes from the ground state, provided we remain nearly adiabatic

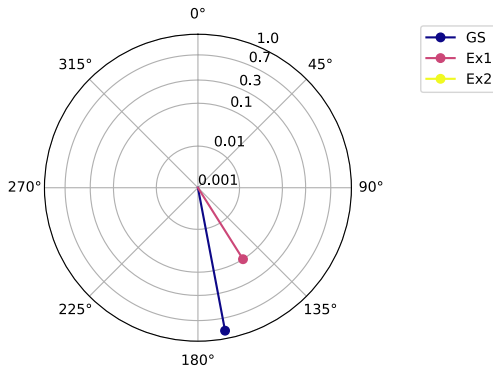


FIG. 4. Exemplary eigenstate clock featuring the complex summands of α for $\tau=1$. Here, the term corresponding to the ground state $|\psi_0|^2 \exp(-iE_0\tau)$ and the first excited state term $|\psi_1|^2 \exp(-iE_1\tau)$ lie quite closely together in phase which leads to problematic constructive interference. However, as the pointers rotate with their respective eigenenergy, they will be well-separated for suitable larger τ . Note that in this instance, the summands corresponding to higher excited states are taken very small and not visible.

throughout the path. We can bound the maximal error in $|\alpha(\tau)|^2$ by computing the average for up to large values of an uniformly distributed τ as

$$E^2 := \lim_{K \rightarrow \infty} \mathbb{E}_{\tau \sim \text{unif. dist. in } [0, K]}(|\alpha(\tau)|^2) = \sum_i |\psi_i|^4. \quad (8)$$

Then, we obtain

$$|\psi_0|^2 \geq \frac{1}{2} + \frac{1}{2} \sqrt{2E^2 - 1} \quad (9)$$

for the ground state population $|\psi_0|^2$. In practice, terms in (Eqn. 7) corresponding to higher eigenenergies will be rather small and destructively interfere with each other.

Therefore, this bound is not tight and much smaller errors are expected in an experiment (cf. App. C4). Our protocol takes inspiration from semi-classical approaches to the quantum phase estimation algorithm [21, 22]. However, these algorithms also seek to determine to energy. As we argued above, the ground state overlap is better suited as the cost function for ground state finding algorithms. Therefore we devised this protocol that is oblivious to the energy value at any given point while being very simple to implement.

B. Entangled-ancillas protocol

Building upon the single-ancilla protocol, we introduce a protocol using two identical quantum systems with one ancilla each. The protocol is motivated by the intuition that the single-ancilla protocol gathers information about the complex phase of $\langle \psi | \psi_{\text{evo}} \rangle$ which is without practical use to us. Instead we would like to estimate $|\alpha|$ directly, which this protocol achieves.

We require the possibility to conduct an entangling measurement (i.e. a Bell measurement) between the two ancillas of the two systems. Such an entangling measurement could be performed with a microwave quantum link between two superconducting circuits [23]. This protocol constitutes an instance of distributed quantum computing for such a quantum network. Moreover, it is well-suited to existing NISQ devices lacking an all-to-all connectivity where the adiabatic evolutions could be implemented on separate but connected sub-graphs [24].

Our goal is to determine the purity of the ancilla. In general, there is the relation $\rho \text{ pure} \Leftrightarrow \text{Tr}[\rho^2] = \lambda_1^2 + \lambda_2^2$ for density matrices, with λ_1 and λ_2 the eigenvalues of ρ . We write the density matrix and its square as

$$\rho_a = \begin{pmatrix} a & b \\ c & d \end{pmatrix} \quad \text{and} \quad \rho_a^2 = \begin{pmatrix} a^2 + bc & \cdot \\ \cdot & bc + d^2 \end{pmatrix} \quad (10)$$

where matrix elements irrelevant for our protocol are denoted with a dot. With the Bell state $|\Phi^-\rangle = (|00\rangle - |11\rangle) / \sqrt{2}$ we construct a Bell measurement. The diagonal matrix elements of ρ_a^2 may then be attained by considering a composite system where the second system has controlled negative time evolution (implementable by changing the sign of H). Then, the density matrix of the ancilla of the second system effectively corresponds to the transpose of the density matrix of the first ancilla $\rho_{a2} = \rho_{a1}^T$. The composite system gives

$$\rho_{a1} \otimes \rho_{a2} = \begin{pmatrix} a^2 & \cdot & bc \\ \cdot & \cdot & \cdot \\ \cdot & \cdot & \cdot \end{pmatrix} = \frac{1}{4} \begin{pmatrix} 1 & \cdot & \cdot & |\alpha|^2 \\ \cdot & \cdot & \cdot & \cdot \\ \cdot & \cdot & \cdot & \cdot \\ |\alpha|^2 & \cdot & \cdot & 1 \end{pmatrix}. \quad (11)$$

If $|\psi\rangle$ is in an eigenstate, the density matrix of the ancilla ρ_a is pure and the expectation of the $|\Phi^-\rangle$ measurement

is

$$\langle \rho_{a1} \otimes \rho_{a2} \rangle_{|\Phi^-\rangle} = \frac{1}{4}(1 - |\alpha|^2) = 0, \quad (12)$$

allowing for very low variance measurements when $|\psi\rangle$ is in the vicinity of the ground state. This protocol is especially well-suited for hypothesis testing (App. F).

V. VARIATIONAL QUANTUM ADIABATIC ALGORITHMS

Preparing the ground state of a Hamiltonian is a problem of great significance in physics with deep implications in the field of combinatorial optimization. While adiabatic state preparation is known to return the ground state for sufficiently long preparation times only, variational quantum algorithms require a very large number of measurements in the training phase. We present a toolbox for variational quantum adiabatic algorithms (VQAA). Our objective is to prepare the ground state of a problem Hamiltonian H_T with high fidelity while keeping the number of measurements in the process as low as possible. We aim at finding an optimized profile for the adiabatic evolution $H(s)$ from the ground state of H_0 to the ground state of H_T . For reasons of completeness, we refer to the Appendix (App. A 1) for a treatment of the adiabatic algorithm and its implementation.

In order to find an optimized adiabatic evolution, we choose a positive resolution $L \in \mathbb{N}$ for this velocity profile and split up the adiabatic path into L chunks. Then, for

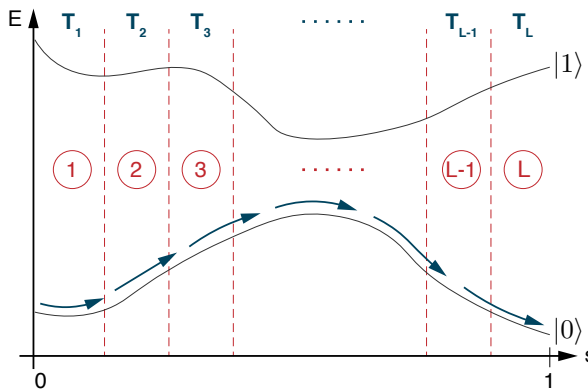


FIG. 5. Illustration of a VQAA by splitting the adiabatic path into L chunks. The ground state and higher excited state energies of $H(s)$ are shown here, being separated by a finite spectral gap. In an adiabatic algorithm, the ground state is prepared by following a path from a trivial Hamiltonian ground state at $s = 0$ to the target Hamiltonian at $s = 1$.

every chunk $i \in \{1, \dots, L\}$ an optimal adiabatic evolution time T_i needs to be determined (Fig. 5).

In every optimization task, keeping the number of parameters to be optimized as low as possible is paramount. This is because every new parameter yields

an additional cost in the number of repetitions necessary to make all the estimations which are required in the optimization of that parameter. In a VQAA, two different options are possible. One could distribute the total time budget T for the evolution from $s = 0$ to $s = 1$ onto the L chunks (e.g. evenly spaced) and optimize the chunk lengths. Or alternatively, one could distribute the chunks in a given way and optimize the T_i . For both options, we present suitable specific algorithms with different resource requirements. An essential ingredient for the algorithms is the ability to obtain information about the closeness of the quantum state at a given point in the adiabatic path with the ground state.

VI. PRESENTATION OF THE ALGORITHMS

The concept for the VQAA allows flexibility in the question of whether the chunk lengths or the chunk evolution times T_i are the parameters to be optimized. Also, different specific classical algorithms can be used for the optimization process. Here, we present three different algorithms for finding the chunk lengths for fixed total evolution time and one algorithm for finding the chunk evolution times for flexible total T . These algorithms have different resource requirements and can make use of different ground state closeness protocols. The results stated in the abstract have been obtained using the gradient-based black box optimization for fixed total time (Sec. VIA 3).

A. Fixed total time optimization

Our proposal for the VQAA allows to set a maximum total time for the adiabatic evolution, which is well-suited for the limitations of current quantum devices. Here, the total adiabatic evolution time T is allocated evenly between the chunks of the adiabatic path, so that

$$T_i = T/L \quad \forall i \in \{1, \dots, L\}. \quad (13)$$

The chunk lengths become the variational parameters to be optimized, effectively controlling the density of adiabatic steps.

1. Ancilla-free optimization for fixed total time

In order to optimize $|\langle \psi(s=1) | \text{GS} \rangle|$, we try to keep the loss in fidelity in the ground state overlap along the adiabatic path as small as possible. Chunk lengths are initialized with equal lengths so that the end positions of each chunk are at

$$s_i = i/L \quad \forall i \in \{1, \dots, L\}, \quad (14)$$

reproducing what we call naive QAA. The chunk lengths are $\bar{s}_i = s_i - s_{i-1}$, with $s_0 = 0$. Then, an adiabatic

evolution is performed from the initial trivial product state $|\psi_0\rangle = |\psi(s=0)\rangle = |-\rangle^{\otimes N}$ up to the end points of each chunk. This adiabatic evolution is then time-reversed (at the same speed) by changing the sign in the unitaries. The total forward and backward time evolution between $s = 0$ and $s = s_i$ are described by $U_{0 \rightarrow s_i}$ and $U_{0 \leftarrow s_i}$, respectively. By going back to the initial product state $|-\rangle^{\otimes N}$, the implementation of this protocol is rather simple and allows for low variance ground state overlap measurements without ancillas. We denote the individual adiabatic evolution operators for chunk j from s_{j-1} to s_j in time T_j with the unitaries $V_{s_{j-1}, s_j}(T_j)$, so that we write

$$U_{0 \rightarrow s_i} = \prod_{j=1}^i V_{s_{j-1}, s_j}(T_j), \quad U_{0 \leftarrow s_i} = \prod_{j=i}^1 V_{s_j, s_{j-1}}(T_j). \quad (15)$$

Now, we compute

$$O_i = |\langle \psi_0 | U_{0 \leftarrow s_i} U_{0 \rightarrow s_i} | \psi_0 \rangle| \quad (16)$$

for all $i \in \{1, \dots, L\}$ with $O_0 = 1$. The consecutive ratios of the overlap are

$$R_i = \frac{O_i}{O_{i-1}} \quad \forall i \in \{i, \dots, L\}. \quad (17)$$

These R_i correspond to the drop in ground state overlap with each next chunk along the adiabatic path. In order to find chunk lengths which correspond to a smooth decrease of the ground state overlaps, chunks i where the drop in ground state overlap is larger than the average

$$R_i > \frac{1}{L} \sum_{i=1}^L R_i \quad (18)$$

are made smaller and vice-versa (where R_j is below average, the j th chunk is made larger). The sum of the chunk lengths is kept normalized to one ($\sum_{i=1}^L \bar{s}_i = 1$). Then, new values O_i are computed and the procedure repeats until convergence.

Clearly, what is optimized here is not exactly the instantaneous ground state overlap because the reversed adiabatic evolution will accumulate extra phases distorting the results slightly. Nevertheless, this method can be a useful compromise between a protocol which is very simple to execute and can still yield improved results of an optimized adiabatic routine (Sec. VII C 2).

2. Forward only evolution for fixed total time

Improving over the ancilla-free algorithm, this algorithm makes use of the ancilla-based ground state closeness protocol (Sec. IV A) in order to estimate the ground state overlap at the point s_i in the adiabatic path

$$O'_i = |\langle \text{GS}_{s_i} | U_{0 \rightarrow s_i} | \psi_0 \rangle| \quad (19)$$

without backwards time-evolution. Here, $|\text{GS}_{s_i}\rangle$ is the instantaneous ground state at point s_i of the adiabatic path. The rest of the procedure is analogue to the previous algorithm. This algorithm enables us to try to keep quantum state along the adiabatic path close to the instantaneous ground state for fixed total adiabatic runtime.

3. Black box optimization for fixed total time

We present a black box optimizer routine which makes use of the gradient to find optimized chunk lengths $\{\bar{s}_i\}$. Here, the chunk lengths are optimized in a quantum-classical feedback loop similar to typical variational quantum algorithms. In our approach, the vector containing the chunk lengths is used as the input for a quantum black box (Fig. 6). The chunk lengths remain normalized to 1. Within the quantum black box, an optimized adiabatic evolution is implemented according to the current chunk length vector, and the output of the black box is the final ground state overlap at $s = 1$. The ground state overlap may be obtained, e.g. by making use of our proposed one-ancilla protocol (Sec. IV A). This value of the ground state overlap is fed into a classical optimizer which updates the input vector. Our cost function is the ground state overlap which we seek to maximize. We use the (quasi-Newtonian) bounded limited memory BFGS (L-BFGS-B) algorithm [25] or the gradient-free Nelder-Mead (or downhill simplex) algorithm [26] for the classical optimization. To make the setting of the optimizer more realistic for an experimental set-up, we fix the relative step size in L-BFGS-B to be larger than 1% of the chunk lengths $\{\bar{s}_i\}$. The feedback loop is repeated until convergence or until another suitable termination criterion is reached, e.g. a desired ground state fidelity.

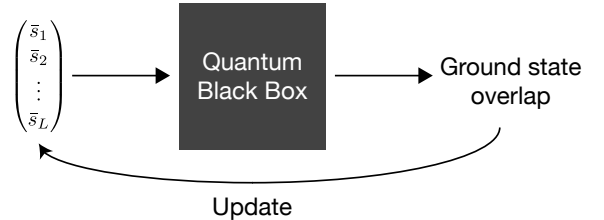


FIG. 6. Quantum classical feedback loop for optimizing the chunk lengths of an adiabatic evolution while keeping the total time fixed. A parameter vector containing the chunk lengths is used as input for a quantum black box. The black box implements an optimized adiabatic evolution accordingly and outputs the ground state overlap. Making use of a classical optimizer, the chunk lengths vector is updated in order to maximize the ground state overlap.

B. Target overlap profile with flexible total time

The concept of the VQAA also allows for flexible total time optimization. Here, the goal is to find an optimized adiabatic evolution which gives a final overlap as close as possible to a given threshold

$$|\langle \psi(s=1) | \text{GS} \rangle| \gtrsim \theta_L, \quad (20)$$

the adiabatic path is split up into L chunks of length s/L with respective evolution times T_i . The state $|\text{GS}\rangle$ is the ground state at the end of the adiabatic path at $s = 1$. By smoothly interpolating from θ_0 at $s = 0$ to θ_L at $s = 1$ the intermediate target thresholds θ_i are set. Starting with the first chunk, we now search for the evolution time T_1 which suffices so that $|\langle \psi(s_1 = 1/L) | \text{GS} \rangle| \gtrsim \theta_1$. Here, we can make use of hypothesis testing which is highly efficient in the number of measurements (App. F). Search algorithms such as bisection methods feature exponentially fast convergence. The $\{T_i\}$ define the optimized adiabatic evolution. This algorithm is then able to follow a target overlap profile with resolution L as closely as possible. We note that due to the limited decoherence time of NISQ devices, a maximal value for the T_i can be fixed.

VII. BENCHMARKING AND RESULTS

For benchmarking purposes, we choose a non-trivial problem where we are able to simulate the evolution of a quantum computer with and without noise on a classical computer. Simulating the dynamics of a large quantum system on a classical computer is, in general, very hard as the number of coefficients necessary for the classical description increases exponentially with the system size N . For this reason, we choose a gapped one-dimensional Hamiltonian as our system. In the algorithms we propose, the state is always close to the ground state, i.e. has few excitations only. The ground states of gapped one-dimensional systems can be described efficiently using a matrix product state (MPS) ansatz. We give a brief outline of the tensor network techniques [27] we use to simulate our algorithms classically in (App. D). Therefore, even though MPS cannot approximate time evolution in general, it is ideally suited for our problem since our states have few excitations.

A. Model

For benchmarking a simple, yet non-integrable quantum model, we use the translationally invariant Ising model with transverse and longitudinal fields, hereafter referred to as the ZZXZ model

$$H_T = \sum_{i=1}^N (J\sigma_i^z\sigma_{i+1}^z + h\sigma_i^x + g\sigma_i^z) \quad (21)$$

as a finite system with open boundary conditions [28]. For $J > 0$ we are considering the antiferromagnetic ZZXZ model. A choice of the coefficient $J = 1$ places the model in the paramagnetic phase (Fig. 7) and an adiabatic

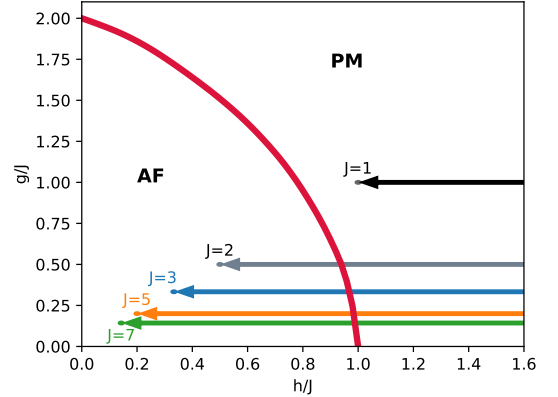


FIG. 7. Zero-temperature phase diagram of the ZZXZ model in the thermodynamic limit. The antiferromagnetic phase (AF) is separated from the paramagnetic phase (PM) by a second-order phase transition (red line). At the multi-critical point at $(h, g) = (0, 2)$ the model becomes classical resulting in a first-order phase transition. For different interaction strengths J the adiabatic evolution follows different paths in the phase diagram. Phase diagram after [29], note that their different Hamiltonian formulation results in an appropriately rescaled phase diagram.

evolution from the trivial Hamiltonian $H_0 = \sum_i h\sigma_i^x$ stays entirely within the paramagnetic phase, therefore no phase transition is crossed [29, 30]. This is different for choices, e.g. $J = \{2, 3, 5, 7\}$, where the adiabatic paths crosses a second-order phase transition from the paramagnetic phase into the antiferromagnetic phase. The adiabatic spectrum following a linear interpolation (subject to a reparametrization $\lambda(s)$, cf. App. A 1) from H_0 to H_T is discrete for the lowest energy eigenstates.

B. Results for adiabatic spectroscopy

We benchmark the adiabatic spectroscopy for the ZZXZ model on a qubit chain with $N = 53$ sites. For our model, the spectral gap $\Delta(s)$ has been obtained using DMRG methods (Fig. 8). In our simulations, we compute the ground state overlap directly using tensor contractions, however, in an experiment, this information would be gathered using our ancilla protocols (Sec. IV). In an experimental setting, every time we would like to make a measurement to estimate $|\alpha(\tau)|$, we can choose to evolve uniformly at random for different values of τ between 0 and some very large K . Under these assumptions a simple analytical formula for the expectation value E^2 of $|\alpha(\tau)|^2$ can be given (App. C 4) and a target ground state overlap of $|\psi_0| = 0.8$ translates

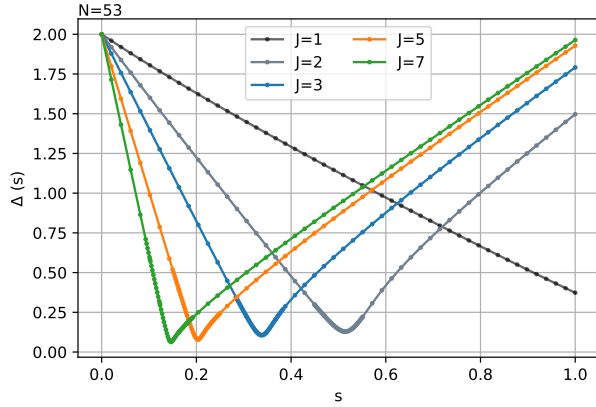


FIG. 8. Spectral gap $\Delta(s)$ for the ZZXZ model $N = 53$ qubits and different values of J , obtained with DMRG methods. The energy difference between the ground state and the first excited state is plotted along the adiabatic path in s . The minimal spectral gap along the adiabatic path is smallest for large interaction strength J and the phase transition is crossed earlier in parametrized time s .

to

$$E^2 := \lim_{K \rightarrow \infty} \mathbb{E}_{\tau \sim \text{unif. dist. in } [0, K]} (|\alpha(\tau)|^2) \geq 0.54. \quad (22)$$

In the adiabatic spectroscopy, we obtain the evolution times $T(s)$ required to reach this target for a given value of s (Fig. 9). Clearly, there is a strong increase in

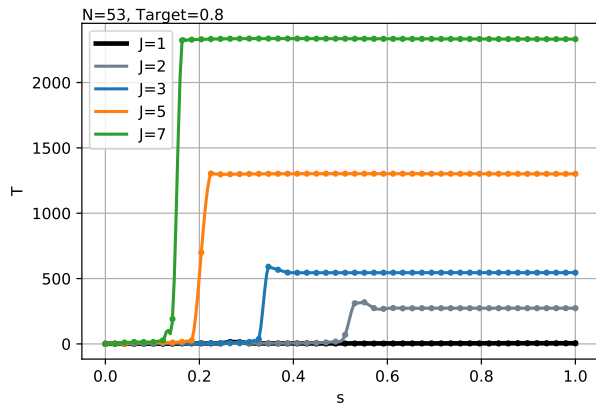


FIG. 9. Adiabatic spectroscopy for $N = 53$ qubits and a given target ground state overlap of 0.8, we perform adiabatic sweeps from 0 to s and find the evolution time T required to reach the target overlap. We obtain data for 50 values of s linearly distributed along the x-axis. When a phase transition needs to be overcome, the T 's rise to much larger values. The steepness of curve at this point provides a measure for the smallness of the spectral gap.

T around the position of the minimal spectral gap for respective J . By computing the derivative of the (cubic) splines, we extract the position and smallness of the gap which correspond to the position and steepness of the T -increase in the $T(s)$ plot. For closer resemblance with

the actual spectral gap profile, we plot $-\partial T(s)/\partial s$ (and clip values above zero) in (Fig. 1).

C. Results for VQAA

Here we compare the benchmarking results obtained for the different algorithms and interpret their respective behavior. In particular we would like to highlight that there are two regimes where an optimized adiabatic path improves over non-optimized (or naive) QAA. When a phase transition is crossed in an adiabatic evolution, as intuition would suggest, optimal adiabatic paths concentrate the majority of the evolution time around the position of the spectral gap. We also examine the case without a phase transition ($J = 1$) and benchmark for systems with up to $N = 100$ qubits. Here, we observe that rotations in the low-energy eigenspace can significantly improve the performance of the quasi-adiabatic evolution. Moreover, we find that leaving the instantaneous ground state can pay off in finding a better final ground state overlap. This seems to be especially significant for short total evolution times.

1. Black box optimization for fixed total time

The best results for fixed time are achieved with the black box algorithm. Even for large system sizes, this algorithm can be able to improve significantly over naive QAA for fixed total time. Good results are usually achieved for a handful of chunks already and the performance of the algorithm does not improve much further for more chunks (which would correspond to a higher resolution in the adiabatic velocity profile). This is the case both when a small spectral gap needs to be crossed, but also in the absence a phase transition. In the latter case, the black box algorithm very often returns an adiabatic path including one or even several very small chunks.

These rotations can be understood in the following way. The set-up of the VQAA with fixed time allows some chunk length \bar{s}_i to become very small. In these small chunks, however, there is still an amount of time T_i spent. The evolution in such a chunk in the limit of $\bar{s}_i \rightarrow 0$ is implemented by a unitary

$$U_{\text{rot}}(T_i, s_i) = e^{-i T_i H(s_i)} \quad (23)$$

which effectively changes the local phases of $|\psi(s_i)\rangle$ thereby physically changing the quantum state. As $|\psi(s_i)\rangle$ in our algorithm is expected to have a considerable ground state population and also small populations in the lowest excited states, the change in the local phases of $|\psi(s_i)\rangle$ corresponds to a rotation in the low energy eigensector. Some rotations eventually become beneficial for the performance of the adiabatic routine.

In the case of a phase transition, the improvement in the evolution time T between naive QAA and an optimized adiabatic evolution is much larger than without a small gap. For very few chunks only, target fidelities of over 90% in a system of 53 qubits were reached at around $T \approx 100$. With a non-optimized adiabatic path, this would have required very long (\approx factor 10 longer) preparation times as depicted in (Fig. 2). The classical optimizer used for obtaining the data in this figure is the Nelder-Mead algorithm. In our simulations, Nelder-Mead proved to be more robust at large T at the expense of requiring more measurements. Being a gradient-free method, we expect it to behave better than the gradient-based L-BFGS-B for noisy systems.

In (Fig. 10), the evolution of the chunk positions for an

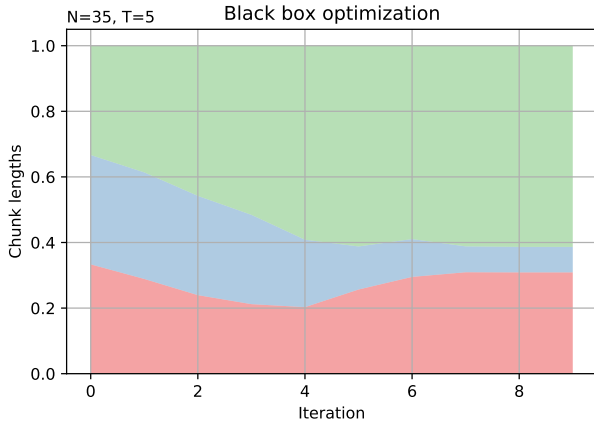


FIG. 10. Instance of a black box optimizer for the case when crossing a phase transition, here for $J = 3$ and $N = 35$. The stacked chunk lengths are shown for the first nine iterations as the middle chunk becomes smaller. This leads to the evolution time being spent effectively around the smallest gap at $s \approx 0.33$.

instance of the black box algorithm is shown for 35 qubits and $J = 3$. Here, the total time is $T = 5$ and L-BFGS-B was chosen as the classical optimizer due to its faster convergence in the classical simulations. The adiabatic spectrum for $J = 3$ features a small gap around $s = 0.33$. This can be approximately captured with three chunks only. Over a few iterations, the center chunk becomes smaller around the position of the gap, so that more time in the adiabatic evolution is spent there.

In the case without a phase transition, for $J = 1$, we find reductions of the total evolution time by a factor of over 3 when comparing with naive QAA. Here, we benchmark the black box optimization routine for large values of T and 100 qubits (Fig. 11). We note that for $T > 40$, the classical L-BFGS-B algorithm was in most cases not able to find an optimized adiabatic path. It was made sure that the reason for this was not due to memory-limitations in the optimizer, the relative step size or tolerance values for the termination of the algorithm. Increasing the number of chunks does not generally help in finding better optimized paths.

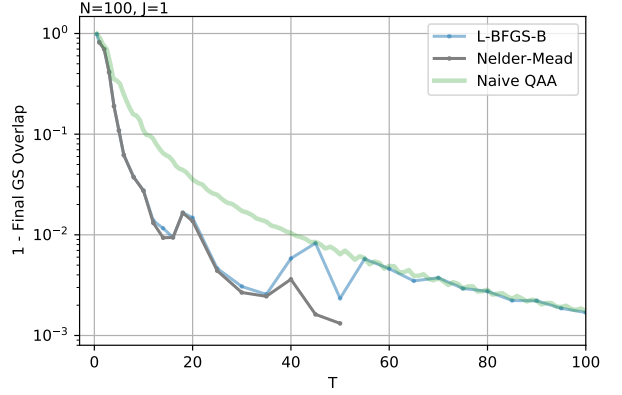


FIG. 11. Large T black box optimizer benchmark for the two classical optimization algorithms L-BFGS-B and Nelder-Mead (NM). Data for was obtained only up to $T = 50$ and requires, in general, more measurements than gradient-based methods. However, the optimization with L-BFGS-B became increasingly unstable for large $T > 40$ and NM was observed to be more robust.

However, sequential initializations of the optimizers can improve the performance. Instead of starting with naive QAA, the optimizer then begins with the chunk lengths of the previous, shorter-time optimizer instance.

A typical black box algorithm instance (for $J = 1$, i.e. no small gap) is shown in (Fig. 12) where the small chunks can be easily observed around $s = 0.34$. Indeed, the ground state overlap is maximized and the energy minimized in five iterations only. In (Fig. 13), the overlap between $|\psi(s)\rangle$ and the ZZXZ ground state or the instantaneous ground state of $H(s)$, respectively, is shown. The exact ground states have been obtained using DMRG methods. A discontinuity in the path of the optimized QAA is clearly visible for $s = 0.34$ due to the implemented rotation. As the black box optimizer only has access to the ground state overlap at $s = 1$, it is agnostic to the actual curve of the optimized QAA for values below $s < 1$. It is interesting to observe that in fact leaving the instantaneous ground state can lead to better final results at $s = 1$, also discussed for adiabatic evolutions in [31] and in a related way in the context of diabatic transitions in QAOA in [32]. This feature can also be observed in a black box optimizer instance for a smaller system in (Fig. 14) where the optimized QAA curve gives a final overlap of approximately 0.999 and recovers most of its ground state overlap in the last 20% of the adiabatic evolution path only.

2. Converging overlap ratios for fixed total time

Besides the black box approach to VQAA, we have presented other algorithms which aim to stay close to the instantaneous ground state along the adiabatic path. Both the ancilla-free and the one-ancilla method seek for convergence in the overlap ratios between consecutive

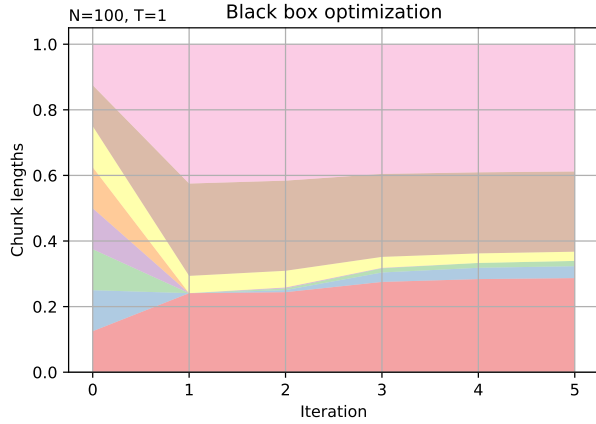


FIG. 12. Stacked chunk lengths adding to $s = 1$ display the evolution of an instance of a black box optimizing routine. Chunks are initialized with equal lengths and their lengths optimized using a L-BFGS-B optimizer with regard to a maximal final fidelity with the ground state of the ZZXZ Hamiltonian. A confluence of chunks around $s = 0.34$ can be observed.

chunks. The one-ancilla method is cleaner in the sense that it directly uses the overlap and does not accumulate extra transitions and phases on the backwards path (Sec. VIA 2). The one-ancilla method can achieve a smooth adiabatic path which remains as close as possible to the ground state at all times for fixed total evolution time. However, the ancilla-free method finds adiabatic paths which effectively implement a rotation in the low energy eigensector. This property is also observed in the gradient-based black box method (Sec. VII C 1) and seems to be very relevant for preparing the ground state on NISQ devices. Therefore the choice of which method of the will perform better is likely quite model-dependent for these two algorithms.

3. Target overlap profile for flexible total time

The flexible total time algorithm with a given target overlap with the ground state at the end of the adiabatic evolution is well-suited in the kind of instances in which staying close to the ground state is desired. As we observe in (Fig. 15) the naive QAA will occasionally leave the ground state leading to oscillations in the instantaneous ground state overlap. Considering the adiabatic path split-up into several chunks, due to the changing Hamiltonian $H(s)$ different evolution times $\{T_i\}$ for each chunk are necessary in order to achieve a given overlap with the ground state at the end of the adiabatic evolution. Values for the $\{T_i\}$ strongly depend on the spectral gap $\Delta(s)$ between the ground state and the excited state as well as on the Berry connections (App. A 2).

We observe that our algorithm is able to reduce the total adiabatic evolution time compared to naive QAA

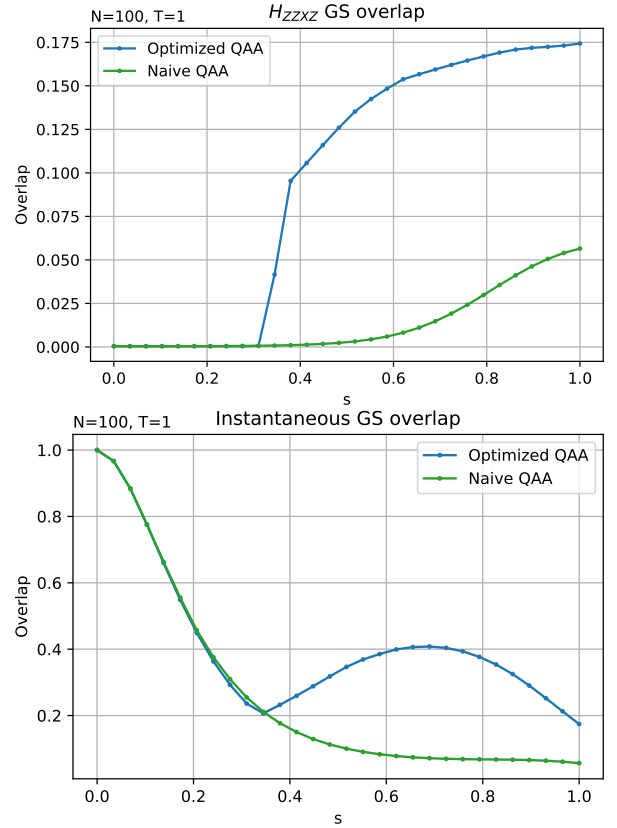


FIG. 13. The ground state overlap is plotted along the adiabatic path for different values of s . The results are for $N = 100$ and fixed total time $T = 1$. The optimized QAA curve (blue) differs significantly from naive QAA (green curve) in the region of very small chunks around $s = 0.34$. Note that the spectral gap between the ground state and the first excited state is not minimal in this region, but decreases strictly monotonically with s . At the end of the evolution, optimized QAA achieves a ZZXZ model ground state overlap of 17.4% while naive QAA results in an overlap of 5.7%.

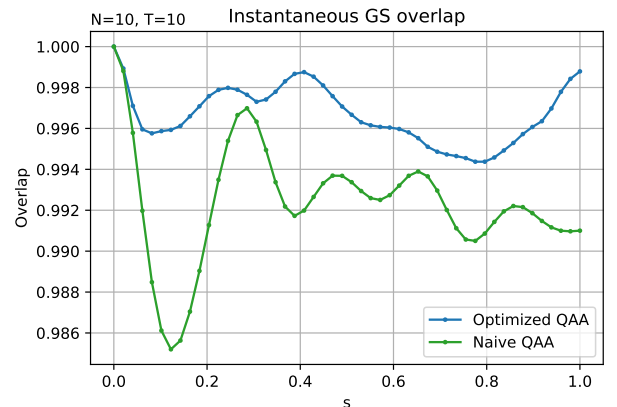


FIG. 14. In this instance, albeit for $N = 10$, we see near perfect ground state preparation for $T = 10$ without increasing the total time budget. Even though the instantaneous ground state overlap with $H(s)$ along the adiabatic path was not very large, the final ground state overlap is 0.999.

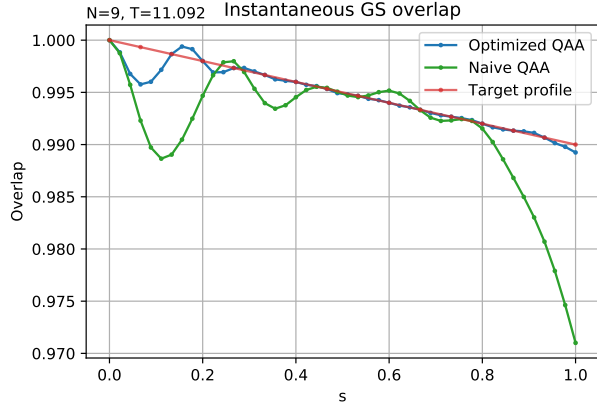


FIG. 15. Instantaneous ground state overlap for QAA optimized with the flexible total time algorithm compared to naive QAA with the same time budget. The target fidelity at $s = 1$ was set to $\theta = 0.99$ and linearly interpolated along the adiabatic path. The search interval for the time spent in each chunk was upper bounded such that $T_i \leq 20 \forall i$.

in this toy example. This is because it uses the time available in a more economic way by spending much of the evolution time only when required to stay close to the ground state. One useful property of this algorithm is the fact that it is self-verifying in a sense that the hypothesis testing at the end of every chunk guarantees with high confidence that the ground-state overlap is larger than a given value. Further developments of this algorithm can be envisioned where the $\{T_i\}$ are optimized to follow a more complicated profile. Moreover, the results of this algorithm serve as a good initial point for the gradient-based black box algorithm for fixed total evolution time. Here, we have set the chunk lengths $\{\bar{s}_i\}$ to equal values. Adoptions of this algorithm with unevenly spaced chunks are also possible. Including additional chunks with very small chunk length could possibly provide a better performance of the algorithm by making it possible to implement rotations in the low energy eigensector at the expense of an increased number of measurements (Sec. VII C 2).

VIII. NUMBER OF MEASUREMENTS

In every variational algorithm, the number of measurements needed in order to obtain satisfactory results is of upmost importance as it directly determines the feasibility of the approach. Here, we discuss the number of measurements necessary for each respective algorithms presented in this paper. We focus on the number of ground state overlap evaluations necessary in our classical simulations. To obtain the ground state overlap from $|\alpha|$, a small overhead is required (Sec. IV A). Both the *ancilla-free* and *one-ancilla fixed time algorithms* converge with very few iterations even for large system sizes ($N = 100$). The resolution of the

velocity profile in the adiabatic evolution is the number of chunks chosen. In our case, the number of ground state overlap evaluations was fairly low with

$$\#\text{GS overlaps} = \#\text{iterations} \cdot \#\text{chunks} \lesssim 100 \quad (24)$$

which sufficed for our simulations. The number of chunks are the number of parameters to be estimated and for the *flexible total time algorithm* this corresponds to the number of bisection searches required. As these search algorithms converge exponentially fast, roughly 10-20 ground state overlap estimations per search are usually sufficient for highest accuracies of the optimized $\{T_i\}$ values. In this algorithm, the two-ancilla algorithm is used which is suitable for hypothesis testing. Hypothesis testing converges exponentially fast as well, asking for about another 10 measurements for each ground state overlap estimation. Exemplary numbers for hypothesis testing are given in the Appendix (App. F).

The *black box algorithm* depends on ground state overlap evaluations in order to estimate the gradient. The number of ground state overlap evaluations necessary in the optimization process is directly related to the number of chunks. Already for very few iterations, good results can be obtained with this method, so that for five chunks, we achieved good results for $N = 100$ and $T = 1$ with significantly less than 50 ground state overlap evaluations in total (App. Fig. 21). For a random variable X with values in $[a, b]$, $\bar{\Delta} = b - a$ and independent and identically distributed samples, the Chernoff-Hoeffding inequality [33] gives an upper bound on the probability to find the measurement deviating more than ϵ from its expectation value μ

$$\Pr(|X - \mu| \geq \epsilon) \leq e^{-2m\epsilon^2/\bar{\Delta}^2} =: \eta \quad (25)$$

For Pauli measurements, we can have either +1 or -1 as results, so $\bar{\Delta} = 2$ and the number of measurements

$$m \geq \frac{2}{\epsilon^2} \log\left(\frac{1}{\eta}\right) \quad (26)$$

depends on the η and ϵ needed. Setting the precision ϵ to $(\#\text{GS overlap})/20$ and the failure probability so that 1 in 2 experiments is successful with all estimations within the deviation ϵ , we estimate the number of measurements necessary to be of the order of 10^3 .

The number of GS overlaps required to reach very high overlaps > 0.9 at larger T is naturally larger than what stated above for $T = 1$. In (Fig. 2), the maximum number of GS overlap evaluations was set to 1000, while typically few hundred evaluations sufficed to find an adiabatic path with maximal ground state overlap up to 10^{-8} relative accuracy. Without doubt, this accuracy will be unattainable in current experiments and much less ground state evaluations give already very good results. In fact, we estimate that for $N = 53$ in the case of a phase transition and $T \approx 100$, when obtaining less than 200 ground state evaluations in the

Nelder-Mead method will yield results of practically the same quality. These estimations suggest considerably low number of measurements even for optimizing the adiabatic evolution of large quantum systems.

IX. NOISE

A. Noise in adiabatic quantum computation

The noise in current quantum devices severely limits the performance of many quantum algorithms [34]. Therefore, we discuss some important properties of noisy quantum adiabatic algorithms. A general inherent robustness of adiabatic evolution has already been established for some time [35], here we focus on a few points that are especially important to our method.

In a gate-model quantum algorithm without error correction, a flipped qubit will in the worst case render the whole quantum computation nonsensical. This is quite different in an adiabatic algorithm as for physical instances low energy spectral lines are rare (App. Fig. 22a). While a flipped qubit in the preparation of the ground state in an adiabatic algorithm can also lead to a quantum state orthogonal to the ground state, the energy, however, of this orthogonal excited state will still be a very good approximation to the ground state energy. Intuitively, one bit flip corresponds to a single excitation of the system. We can therefore assume that errors increase the energy only by $\mathcal{O}(1)$ for fixed time, when flipped qubits are rare. Also, the position s_0 in the adiabatic path, where a flipped qubit occurs, is not critical. (App. Fig. 22b). This may seem somehow surprising, but it can be explained because a perfect adiabatic evolution suppresses all transitions between the eigenstates. It does not only apply to the ground state but also to excited states. Therefore, a noise-induced excitation will in the regime of an adiabatic evolution not lead to further deviations from the ground state energy.

However, for time evolutions that are faster than an adiabatic evolution, which is in general the case on quantum devices limited in coherence time, we would generally expect light-cone spreading of noise through the spin-chain. Yet, in our simulations this was not observed to be problematic for the performance of the VQAA. In general, the noise behavior of adiabatic algorithms is encouraging as it suggests very benign noise features in these kind of algorithms making them a suitable candidate for NISQ devices.

B. Impact of noise in the presented algorithms

Here, we include a qualitative discussion about the expected performance of the algorithms presented in this paper in the presence of noise. We expect the *adiabatic spectroscopy* to be quite robust to noise as the

information obtained using this method relies on multiple data points and a rather distinctive feature in the $T(s)$ curve resulting from a small spectral gap. Noise effects will become stronger towards the end of the adiabatic evolution as noise accumulates in the circuit. However, as the results of this spectroscopy are quite pronounced, a qualitative description of the gap is likely only slightly impaired by moderate noise in the circuit.

Regarding the *VQAA algorithms*, when considering noise, there are two main points to consider. First, noise can substantially impede the training phase of the algorithm, when the parameters of an optimal adiabatic path are being searched for. Second, in order to prepare the ground state with a desired high fidelity, an adiabatic evolution time T that is only a fraction of the T required for naive QAA suffices with an optimal adiabatic path. This may help strongly in suppressing errors.

Following a target profile is especially tricky when noise comes into play. This is because noise strongly alters the required target profile and we do not expect this method to be very robust to noise. For the black box method, in classical simulations with noise, we observed the gradient-based training to be not too well-behaving. Convergence to optimized paths that improve over naive QAA was often impossible even when only few bit flips occurred in the quantum circuit. Classical optimization routines which are more robust towards noise seem to be asked for here, i.e. a classical optimizer that is combined with an error mitigation technique so that noisy outputs of the quantum black box can be corrected. We note,

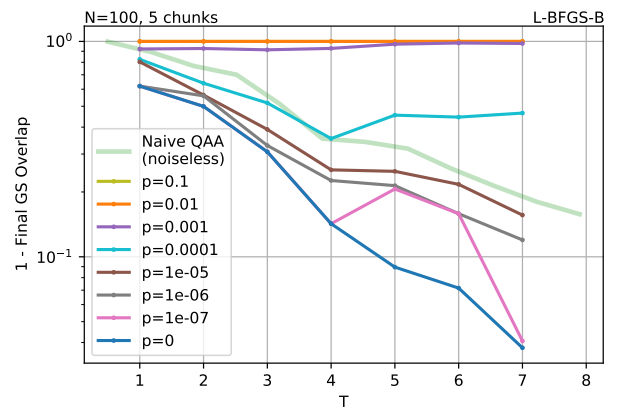


FIG. 16. Noisy benchmark of the black box algorithm for $N = 100$, $J = 1$ and a maximum of 7 optimizer iterations. The noise strength p determines the expected number of noisy qubits. Noise is applied in the circuit both in training as in the testing phase. Note that the behaviour of the pink curve ($p = 10^{-7}$) can be explained due to the very rare noise events, e.g. for $T = 5$ a single adiabatic evolution will see a noisy qubit with average probability of ≈ 0.1 (cf. App. D 2). No measurement noise was considered and naive QAA is given as a reference without noise. L-BFGS-B was used as the classical optimizer.

that the Nelder-Mead algorithms is expected to be more robust to noisy environments and could provide better

performance in an experimental setup than a gradient-based method. In (Fig. 16), it can be observed that small amounts of noise significantly impair the training process of an optimized adiabatic path. For small noise strengths p , however, the results can improve even over naive QAA. For simulating the noisy quantum circuit, 100 MPS samples were taken. We refer to the Appendix for more details on the noise model (App. D 2).

A further comment shall be specifically addressing the noise in the black box algorithm which makes use of a gradient to optimize the adiabatic path. In a recent work, it has been shown that the gradient in a variational quantum algorithm vanishes exponentially in the number of qubits N when the number of layers scales as $\text{poly}(N)$ [14]. These noise-induced barren plateaus severely hinder the scalability of variational quantum algorithms on NISQ devices. In our work, however, the algorithms either optimize the adiabatic path for fixed total evolution time (which includes the gradient-based black box algorithm), or have a maximum time budget in the case of the target overlap profile algorithm. Thus, the (maximum) circuit depth is fixed in our approach which makes the results on noise-induced barren plateaus not directly applicable.

X. DISCUSSION

In this paper, we present a toolkit for quantum adiabatic computation. This toolkit includes a proposal for adiabatic spectroscopy, ancilla protocols for estimating the ground state overlap as well as the VQAA as a flexible yet powerful framework for variationally optimized adiabatic paths for high-fidelity ground state preparation.

The adiabatic spectroscopy offers a straightforward approach to obtain information about an adiabatic spectrum. Our method relies on protocols to evaluate the closeness of an N -qubit quantum state $|\psi\rangle$ to an eigenstate using controlled unitary evolution. By remaining sufficiently adiabatic throughout the evolution, a self-consistent argument applies, enabling us to identify this eigenstate with the ground state. We note, that the error in the ancilla protocols presented is smallest when being close to an eigenstate. The protocol which we propose requires the ability to implement controlled time evolution on a single ancilla qubit. Current technology already meets the requisites of our protocol: Conditional dynamics have been explored in the context of trapped ion simulators and Rydberg atom arrays [36, 37] and they can be implemented efficiently in a gate model.

A natural requirement for the spectroscopy is that the decoherence time of the quantum device is not a limiting factor to determine the evolution time required in order to reach the target overlap. The applications of the adiabatic spectroscopy go beyond obtaining the spectral gap for a given Hamiltonian $H(s)$. By aggregating

spectral information from several adiabatic paths which cut through the phase diagram of a target Hamiltonian H_T , rich properties of quantum many-body systems might be acquired.

We shall now discuss the VQAA from two perspectives. First, the perspective of VQAA as a quantum algorithm for optimal adiabatic paths, and second, VQAA as a variational quantum algorithm which requires only few measurements.

Adiabatic quantum computation is known to prepare the ground state of target Hamiltonian H_T for sufficiently long preparation time T . However, T scales as a function of the minimal spectral energy gap $\Delta(s)$. For general H_T , the best rigorous bound on T has a inverse cubic gap dependence $T = \mathcal{O}((\min_s \Delta(s))^{-3})$ [38]. Due to the limited decoherence time of NISQ devices, large evolution times necessary for high-fidelity ground state preparation can be a difficulty. If it was possible to reduce T to fit into the coherent time frame of a quantum device, it would become possible to adiabatically prepare ground states, e.g. the solution of an optimization problem, that have remained unattainable before.

The question of finding an optimal path for the adiabatic evolution has been in the focus of research efforts for several years already and for the problem of an unstructured search, Grover-type speed-ups have been shown [39, 40]. However, the position and size of the spectral gap are a priori unknown, and obtaining the spectral properties of the adiabatic path can be as hard a problem as preparing the ground state. Therefore, it remains a challenge how an optimized adiabatic path can be obtained when no or only little spectral information is available. One recent work employed techniques from reinforcement learning to find an optimal adiabatic path [41]. In our work, we phrase the problem of finding an optimized adiabatic path as a problem to be solved through a variational quantum algorithm with step-wise adiabatic velocity profile.

Turning now towards a discussion of the VQAA as a variational algorithm, we begin by noting that the ground state overlap can be a suitable cost function for quantum-classical feedback loops. Variational approaches such as the quantum approximate optimization algorithm (QAOA) [13] sparked intensive research interest in recent years. The number of measurements necessary to estimate an objective function scales with $\mathcal{O}(\epsilon^{-2})$, where ϵ is the maximum error that can be tolerated in the optimization process. The proposal of the VQAA aims to reduce the number of measurements by requiring relatively fewer parameters that need to be optimized and by considering a cost function with a low variance. Variational approaches for preparing a ground state generally make use of the energy as a cost function and that energy is estimated via the local observables that compose the Hamiltonian [42]. As the actual ground state will generally not be an eigenstate of the Hamiltonian local terms (e.g. if there is frustration), a low variance in the estimates cannot be guaranteed.

Moreover, the orthogonal eigenstates in the low-energy sector typically yield similar energy values, hindering convergence to the ground state. If we were indeed able to directly measure in the eigenbasis of the Hamiltonian at a given point in the adiabatic path, we would seek to exploit the property of proximity to an eigenstate, which is inherent to adiabatic algorithms. The textbook approach for this problem would be a quantum phase estimation (QPE) algorithm, and direct implementation requires an ancilla overhead [18]. Recent semi-classical approaches are able to use a single ancilla only by utilising post-processing schemes [21, 22]. For the VQAA, we suggest the overlap with the ground state as a figure of merit. In the case of the adiabatic algorithm, the optimal value of some other figures of merit, such as the energy, are not directly accessible. Therefore, we present two protocols to evaluate the closeness to an eigenstate using controlled unitary evolution. The entangled ancilla protocol offers the possibility to perform low-variance measurements by harnessing the power of hypothesis testing when being close to an eigenstate. We note that in the case of a small spectral gap, e.g. when a phase transition is crossed, the ground state overlaps are in general very small and special care is needed to extract useful information with the ancilla protocol.

In the limit of very large depth, QAOA recovers a trotterized adiabatic evolution. Therefore, a black box VQAA algorithm bears some similarities to QAOA. Several key differences are remarked though. First, analog to the evolution times in a (trotterized) adiabatic evolution, the unitaries in QAOA feature *angles* as parameters. However, for a quantum cost function H_T , the optimized angles could be too large for the decoherence limit of the NISQ device which the algorithms is supposed to be implemented on. On the contrary, limiting the maximum angles could be rather problematic for the performance of QAOA. This issue does not arise in the black box VQAA as the total evolution time has been fixed. Second, even for large system sizes with 53 or 100 qubits, VQAA significantly improves over naive QAA for a very small number of parameters L only. In QAOA, it is generally expected that deep circuits are necessary to obtain good results for large systems. Finally, even for very small L , the performance of VQAA is lower bounded by the QAA with a linear time profile. This is true for QAOA only when the angles are initialized akin to a trotterized adiabatic evolution which requires large depth QAOA.

XI. SUMMARY AND OUTLOOK

We seek to combine the best from two worlds by combining the strengths of the adiabatic and the variational approaches. We present a toolbox for VQAA building upon ancilla-based methods to evaluate the ground state fidelity at any point in the adiabatic path. Our approach only obtains information about

the proximity to the ground state and is deliberately oblivious to the actual value of the energy throughout the adiabatic path. Due to the small parameter space and the ground state overlap as our cost function, the number of measurements necessary in the optimization of the adiabatic evolution is dramatically lower than for typical variational quantum algorithms such as QAOA. On the whole, our work suggests that a further exploration of NISQ algorithms based on variational adiabatic concepts is indicated.

For instance, there seems to be room for sequential VQAA algorithms. In some instances, when going towards larger T , the black box VQAA does not improve in a strictly monotonous manner. By reusing information from shorter T , the optimized paths for larger T might be improved and obtained more rapidly. In a similar direction, it would be interesting to see how the information gathered through adiabatic spectroscopy will be used for the optimal adiabatic path in an experimental setting. If it was possible to use adiabatic spectroscopy to eliminate or drastically reduce the quantum-classical training phase of VQAA, this would surely be a large advancement in NISQ algorithms for ground state preparation. Also, it remains to be seen, what bounds can be established on how quickly and closely VQAA can find an adiabatic path which is optimal.

Furthermore, there is increasing research interest in error mitigation techniques for NISQ devices [43, 44], and a further exploration of how VQAA might benefit from these techniques appears promising. More generally, the protocols for estimating the ground state overlap presented in this work could make a wide range of new, exciting quantum algorithms for ground state preparation possible. This might include the opportunity for an algorithm to find optimized adiabatic paths using techniques from reinforcement learning or a combination of the protocols with techniques such as projected measurements and the quantum Zeno effect [45]. Besides, in the regime where the time evolution is not strictly adiabatic, high final ground states fidelities might be achieved by not starting in the ground state of the initial Hamiltonian but in an appropriate superposition in the low energy sector of the initial Hamiltonian.

ACKNOWLEDGMENTS

The authors thank M.C. Bañuls, T. O’Brien, S. Lu, D. Wild, A. Sauer and F. Pollmann for insightful discussions. We acknowledge support from the ERC Advanced Grant QUENOCOBA under the EU Horizon 2020 program (grant agreement 742102) and from the Deutsche Forschungsgemeinschaft (DFG, German Research Foundation) under the project number 414325145 in the framework of the Austrian Science Fund (FWF): SFB F7104. BS was supported by the German Academic Scholarship Foundation (Studienstiftung des deutschen Volkes).

Appendix A: Quantum algorithms

1. Implementing the Quantum Adiabatic Algorithm

For a quantum state $|\psi(t)\rangle$ and a Hamiltonian $H(t)$, the time evolution of the state is given by the Schrödinger equation

$$i\frac{\partial}{\partial t}|\psi(t)\rangle = H(t)|\psi(t)\rangle \quad (\text{A1})$$

where we set the reduced Planck constant to $\hbar = 1$. The quantum adiabatic algorithm [8] describes how to prepare the unitaries that implement the path

$$H(s) = (1-s)H_0 + sH_T \quad (\text{A2})$$

from a trivial Hamiltonian H_0 to the problem Hamiltonian H_T . Here, s is parametrized time $s = t/T$ for a total evolution time T . From (Eqn. A1) we have the unitary time evolution operator $U_{T,0}$ which implements

$$|\psi(T)\rangle = e^{-i\int_0^T H(t)dt}|\psi(0)\rangle = U_{T,0}|\psi(0)\rangle. \quad (\text{A3})$$

On gate-model quantum computers, the adiabatic evolution needs to be approximated by discrete adiabatic steps. We write the unitary operator $U_{T,0}$ as a product of M unitaries

$$U_{T,0} = U_{T,T-\delta}U_{T-\delta,T-2\delta}\dots U_{\delta,0} \quad (\text{A4})$$

with $\delta = T/M$. Here, we approximately assume the Hamiltonian $H(s)$ to be fixed in time during a time interval δ :

$$U_{(l+1)\delta,l\delta} \approx e^{-i\delta H(l\delta)} \quad (\text{A5})$$

for $l \in \{0, 1, \dots, M-1\}$. In [8], the maximal size of δ is bounded as $\delta \ll 1/\|H_T - H_0\|$ in order for the approximation to be valid. However, we found a time step $\delta = 1/16 = 0.0625$ to give sufficient accuracy for our simulations (cf. [46]). In the adiabatic approximation, higher order corrections can be partially suppressed by using a reparametrization with smooth derivatives (corresponding to the Hamiltonian being in a Gevrey class as a function of time). We therefore use the smooth parametrization which removes discontinuities in the derivatives at the beginning and end of every chunk

$$\lambda(s) = \lambda_0 + (\lambda_f - \lambda_0) \sin^2\left(\frac{\pi}{2} \sin^2\left(\frac{\pi s}{2}\right)\right) \quad (\text{A6})$$

where $\lambda_0 = s_0$ and $\lambda_f = s_f$ are initial and final time values, respectively of a chunk. In order to ease notation, this reparametrization of s is implicitly understood in the following sections.

In order to apply a time evolution unitary operator $U(\delta, s)$, we make use of the second-order Suzuki-Trotter approximation [47]

$$U(\delta, s) = e^{-i\delta H(s)} \approx \left(e^{-i\delta H(s)_{\text{even}}/(2K)} e^{-i\delta H(s)_{\text{odd}}} e^{-i\delta H(s)_{\text{even}}/(2K)} \right)^K \quad (\text{A7})$$

with $H(s) = (1 - \lambda(s))H_0 + \lambda(s)H_T$. Here, $K = 2$ has proven to be sufficient without any practical decrease in accuracy [46].

In our implementation of time evolution, we truncate singular values after every application of a two-site gate and renormalize the singular values in order to keep the MPS normalized. We monitor the loss in accuracy by keeping track of the norm of the MPS throughout the real time evolution. In general, we aim for a norm error of not larger than 1%. Exact ground states and excited states for benchmarking purposes are obtained using density-matrix renormalization group (DMRG) methods [48, 49]. The code for the classical simulation was written in Python, building upon the blueprint [50] as a basic building block.

2. Theoretical aspects of an adiabatic evolution

Here we outline the main concepts of a theoretical treatment of adiabaticity. When considering transitions from the ground state to the excited states, the spectral gap between the ground state and the first excited state is of

the greatest importance. Notably, the accumulation of relative phases plays a crucial role as well. We derive the differential equations governing the time evolution of a quantum state. Here, we follow the calculations given in [51], yet it is instructive to use parametrized time $s = t/T$ instead of real time t .

Then, the time-dependent and time-independent Schrödinger equations with $\hbar = 1$ are given by

$$i \frac{\partial}{\partial s} |\psi(s)\rangle = TH(s) |\psi(s)\rangle, \quad (\text{A8})$$

$$H(s) |k(s)\rangle = E_k(s) |k(s)\rangle, \quad (\text{A9})$$

respectively. The $|k(s)\rangle$, $k \in [0, n]$, are the eigenvectors of $H(s)$ and the eigenenergies $E_n(s)$ are for simplicity of exposition assumed to be non-degenerate and distinct. $E_0(s)$ is the ground state energy at a given s . We use the representation for a quantum state

$$|\psi(s)\rangle = \sum_k c_k(s) e^{-iT \int_0^s E_k(\tau) d\tau} |k(s)\rangle = \sum_k c_k(s) e^{-iT\phi_k} |k(s)\rangle, \quad (\text{A10})$$

writing $\phi_k = \int_0^s E_k(\tau) d\tau$, and insert it into the time-dependent Schrödinger equation (Eqn. A8)

$$\sum_k \left[\dot{c}_k(s) e^{-iT\phi_k} |k(s)\rangle - iTE_k(s) c_k(s) e^{-iT\phi_k} |k(s)\rangle + c_k(s) e^{-iT\phi_k} |\dot{k}(s)\rangle \right] \quad (\text{A11})$$

$$= -iT H(s) \sum_k c_k(s) e^{-iT\phi_k} |k(s)\rangle, \quad (\text{A12})$$

where the dot denotes the derivative with respect to parametrized time:

$$\dot{c}(s) = \frac{\partial}{\partial s} c(s). \quad (\text{A13})$$

The second term on the left hand side and the right hand side of (Eqn. A12) vanish as $|\psi(s)\rangle$ satisfies the time-independent Schrödinger equation (Eqn. A9), which gives us

$$\sum_k \left[\dot{c}_k(s) e^{-iT\phi_k} |k(s)\rangle + c_k(s) e^{-iT\phi_k} |\dot{k}(s)\rangle \right] = 0. \quad (\text{A14})$$

Multiplying (Eqn. A14) by the state $\langle m(s)|$ from the left yields

$$\sum_k \left[\dot{c}_k(s) e^{-iT\phi_k} \underbrace{\langle m(s)|k(s)\rangle}_{\delta_{mk}} + c_k(s) e^{-iT\phi_k} \langle m(s)|\dot{k}(s)\rangle \right] = 0 \quad (\text{A15})$$

and we obtain

$$\dot{c}_m(s) e^{-iT\phi_m} = - \sum_k c_k(s) e^{-iT\phi_k} \langle m(s)|\dot{k}(s)\rangle. \quad (\text{A16})$$

Then, the system of differential equations for the coefficients to describe the quantum state is given by

$$\dot{c}_m(s) = - \sum_k c_k(s) \exp \left(-iT \int_0^s (E_k(\tau) - E_m(\tau)) d\tau \right) \langle m(s)|\dot{k}(s)\rangle \quad \forall m \in [0, n]. \quad (\text{A17})$$

The $i \langle m(s)|\dot{k}(s)\rangle$ are also referred to as the Berry connections [52].

From the time-independent Schrödinger equation (cf. Eqn. A9), by taking the time-derivative, we obtain

$$\dot{H}(s) |k(s)\rangle + H(s) |\dot{k}(s)\rangle = \dot{E}_k(s) |k(s)\rangle + E_k(s) |\dot{k}(s)\rangle \quad (\text{A18})$$

and by multiplying with $\langle m(s)|$ from the left, we get

$$\langle m(s)|\dot{k}(s)\rangle = \frac{1}{E_k(s) - E_m(s)} \langle m(s)|\dot{H}(s)|k(s)\rangle. \quad (\text{A19})$$

Under the adiabatic approximation we consider the evolution generated by $H(s)$ adiabatic if the changes of $H(s)$ are very slow compared to the time scale of the system, where the time scale ΔT_{km} is defined as the characteristic time of transition between the k th and the m th eigenstate:

$$|\langle m(s)|\dot{H}(s)|k(s)\rangle| \ll \frac{E_k(s) - E_m(s)}{\Delta T_{km}}. \quad (\text{A20})$$

In the adiabatic limit of infinitely slow change in $H(s)$, we have

$$\lim_{\Delta T_{km} \rightarrow \infty} \langle m(s)|\dot{k}(s)\rangle = 0, \quad m \neq k. \quad (\text{A21})$$

Then, in the adiabatic limit, (Eqn. A17) reads

$$\dot{c}_m(s) = -c_m(s) \langle m(s)|\dot{m}(s)\rangle \quad (\text{A22})$$

with $\dot{c}_m(0) = \delta_{nm}$, i.e. at the beginning of the evolution the whole population is in the n th eigenstate and will strictly remain in this eigenstate subspace if the evolution is perfectly adiabatic. For $n = 0$ we have the special case of the QAA: if a (perfect) adiabatic evolution starts in the ground state, the initial state will remain in the instantaneous ground state subspace until the target Hamiltonian is reached at $s = 1$.

3. Variational algorithms and parametrized circuits

The concept of a parametrized circuit is to write a trial wavefunction which approximates the desired quantum state. This trial state is prepared as a product of many unitary operators, of which each depends on a classical variational parameter acting upon an initial trivial state. The operator preparing this state can be written as

$$U(\varphi) = U_L(\varphi_L) \cdots U_2(\varphi_2) U_1(\varphi_1) \quad (\text{A23})$$

where the $\{\varphi_i\}$, $\forall i \in \{1, \dots, L\}$, are vectors of continuous parameters. The performance depends strongly on the

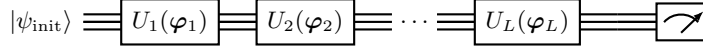


FIG. 17. Quantum circuit for a parametrized circuit. Multiple parametrized unitaries act upon a trivial initial state. Our diagrams were created using the Quantikz package [53].

details of the target Hamiltonian and appropriate parameter initialization can be necessary, albeit is ultimately not sufficient due to the dependence of the algorithm performance on the representative power of the chosen ansatz $U(\varphi)$.

4. The quantum approximate optimization algorithm

The quantum approximate optimization algorithm (QAOA) [13] is a highly popular example of a parametrized ansatz and much research has been done at investigating the properties of this algorithm [32]. We outline QAOA here:

Starting with an initial spin state [54]

$$|\psi_{\text{init}}\rangle = |+, \dots, +\rangle = \frac{1}{\sqrt{2^N}}(|\downarrow\rangle + |\uparrow\rangle)^{\otimes N}, \quad (\text{A24})$$

we write down the QAOA ansatz

$$|\psi_p(\gamma, \beta)\rangle = e^{-i\beta_p H_0} e^{-i\gamma_p H_T} \dots e^{-i\beta_1 H_0} e^{-i\gamma_1 H_T} |\psi_{\text{init}}\rangle \quad (\text{A25})$$

where $\beta = (\beta_1, \dots, \beta_p)$, $\gamma = (\gamma_1, \dots, \gamma_p)$ with integer $p \geq 1$. H_0 and H_T are non-commuting Hamiltonians. $H_0 = \sum_{j=1}^N \sigma_j^x$ is also called the mixing Hamiltonian and H_T is the problem Hamiltonian. In the usual case, H_T is diagonal in the computational basis and encodes combinatorial optimization problems, e.g. MAX-CUT, 3SAT, etc.

The energy cost function

$$E_p(\gamma, \beta) = \langle \psi_p(\gamma, \beta) | H_T | \psi_p(\gamma, \beta) \rangle \quad (\text{A26})$$

is determined with a quantum device by repeated measurements in the computational basis. Using a classical computer, the energy is then variationally minimized towards a local minimum $E_p(\gamma^*, \beta^*)$.

Appendix B: Adiabatic state preparation in the Landau-Zener model

We seek to better understand adiabatic spectroscopy as presented in the main text. Therefore, we would like to obtain a qualitative relation between the spectral gap $\Delta(s)$ along the adiabatic path and the evolution time $T(s^*)$ required to prepare the ground state of $H(s^*)$ with a given target fidelity. In order to do so, we turn towards the well-known Landau-Zener (LZ) model which describes a simple two-level system [55, 56]. The model Hamiltonian is given as

$$H = \lambda(t)\sigma^z + g\sigma^x = \begin{pmatrix} \lambda(t) & g \\ g & -\lambda(t) \end{pmatrix}. \quad (\text{B1})$$

With $\tan \theta = g/\lambda(t)$, we write the eigenvectors as

$$|a\rangle = \begin{pmatrix} \sin(\theta/2) \\ -\cos(\theta/2) \end{pmatrix} \quad \text{and} \quad |b\rangle = \begin{pmatrix} \cos(\theta/2) \\ \sin(\theta/2) \end{pmatrix}. \quad (\text{B2})$$

The eigenenergies are given as $E_{\pm} = \pm\sqrt{\lambda(t)^2 + g^2}$ and the coupling is assumed to be a linear function in time $\lambda(t) = \delta t$. This implies that the minimum of the spectral gap (the avoided level-crossing) is found at $t = 0$, i.e. an adiabatic evolution parametrized by s from 0 to the position of a small gap s^* is understood to be mapped onto the LZ evolution from very small initial t to $t = 0$.

A perturbative approach yields the probability

$$|\alpha_+(t_f)|^2 \approx \frac{\delta^2}{16g^4} \left(\frac{g^6}{(g^2 + \lambda(t_i)^2)^3} + \frac{g^6}{(g^2 + \lambda(t_f)^2)^3} \right) \quad (\text{B3})$$

to find the system in the excited state at t_f after initializing in the ground state at t_i [57]. Assuming the beginning of the adiabatic evolution at $t_i = -\infty$, we are given

$$|\alpha_+(t_f)|^2 \approx \frac{\delta^2}{16g^4} \frac{g^6}{(g^2 + \lambda(t)^2)^3} = \frac{\delta^2 g^2}{16E_+(t)^6} \quad (\text{B4})$$

where we identified t with t_f . Now, we set a target fidelity $A_+^2 := |\alpha_+(t)|^2$ and assume that the total evolution time T scales as $T \sim 1/\delta$:

$$T \sim \frac{1}{\delta} \approx \frac{g}{4A_+E_+(t)^3}. \quad (\text{B5})$$

As we are interested in the change of T , we compute the time-derivative of T

$$\dot{T} \sim -\frac{3}{4} \frac{g\delta}{A_+E_+(t)^5} = -3 \frac{1}{E_+(t)^2} \quad (\text{B6})$$

where we used (Eqn. B5) in (Eqn. B6). Because of $\Delta(t) = 2E_+(t)$ in the LZ model, we obtain $\dot{T} \sim 1/\Delta(t)^2$ as an approximation to the scaling of \dot{T} up to coefficients and possible corrections.

Appendix C: Calculations for the one-ancilla and entangled-ancillas protocol

1. Single-ancilla protocol

The combined system after the unitary evolution can be written as

$$\text{C-}U |\psi\rangle |+\rangle = \frac{1}{\sqrt{2}} [|\psi\rangle |0\rangle + U|\psi\rangle |1\rangle] =: |\zeta\rangle. \quad (\text{C1})$$

Denoting the quantum state after the unitary evolution as $|\psi_{\text{evo}}\rangle = U|\psi\rangle$, we note the following relationships regarding Pauli measurements of the ancilla

$$\langle \zeta | \mathbb{1} \otimes \sigma_x | \zeta \rangle = \frac{1}{2} [\langle 0 | \langle \psi | U | \psi \rangle | 0 \rangle + \langle 1 | \langle \psi | U^\dagger | \psi \rangle | 1 \rangle] = \frac{1}{2} [\langle \psi | \psi_{\text{evo}} \rangle + \langle \psi_{\text{evo}} | \psi \rangle] = \text{Re}(\langle \psi | \psi_{\text{evo}} \rangle) \quad (\text{C2})$$

and

$$\langle \zeta | \mathbb{1} \otimes \sigma_y | \zeta \rangle = \frac{i}{2} [\langle 0 | \langle \psi | U | \psi \rangle | 0 \rangle - \langle 1 | \langle \psi | U^\dagger | \psi \rangle | 1 \rangle] = \frac{i}{2} [\langle \psi | \psi_{\text{evo}} \rangle - \langle \psi_{\text{evo}} | \psi \rangle] = -\text{Im}(\langle \psi | \psi_{\text{evo}} \rangle) \quad (\text{C3})$$

so that

$$\langle \psi | \psi_{\text{evo}} \rangle = \langle \sigma_x - i\sigma_y \rangle_{\text{ancilla}} = \left\langle \begin{pmatrix} 0 & 0 \\ 2 & 0 \end{pmatrix} \right\rangle_{\text{ancilla}}. \quad (\text{C4})$$

For a fixed Hamiltonian $H = \sum_j E_j |\phi_j\rangle \langle \phi_j|$ with the unitary $U |\phi_j\rangle = e^{-iH\tau} |\phi_j\rangle = e^{-iE_j\tau} |\phi_j\rangle$, we write the state $|\psi\rangle = \sum_j \psi_j |\phi_j\rangle$ in the eigenbasis of H with $|\psi\rangle$ normalized ($\sum_j |\psi_j|^2 = 1$). The total quantum system can be expressed as

$$|\zeta\rangle = \frac{1}{\sqrt{2}} [|\psi\rangle |0\rangle + U |\psi\rangle |1\rangle] \quad (\text{C5})$$

$$= \frac{1}{\sqrt{2}} \left[\left(\sum_j \psi_j |\phi_j\rangle \right) |0\rangle + \left(\sum_j e^{-iE_j\tau} \psi_j |\phi_j\rangle \right) |1\rangle \right] \quad (\text{C6})$$

$$= \frac{1}{\sqrt{2}} \left[\sum_j \psi_j |\phi_j\rangle \left(|0\rangle + \sum_j e^{-iE_j\tau} |1\rangle \right) \right] \quad (\text{C7})$$

which we now use to calculate the density matrix of the ancilla qubit

$$\rho_{\text{ancilla}} = \text{Tr}_{\text{non-ancilla}} (|\zeta\rangle \langle \zeta|) = \frac{1}{2} \sum_{j,m} \text{Tr}_{\text{non-ancilla}} \left(\psi_j \psi_m^* \underbrace{[|\phi_j\rangle \langle \phi_m|]}_{\delta_{j,m}} [|0\rangle + e^{-iE_j\tau} |1\rangle] [|0\rangle + e^{iE_m\tau} \langle 1|] \right) \quad (\text{C8})$$

$$= \sum_j \frac{|\psi_j|^2}{2} [|0\rangle + e^{-iE_j\tau} |1\rangle] [\langle 0| + e^{iE_j\tau} \langle 1|] \quad (\text{C9})$$

$$= \sum_j \frac{|\psi_j|^2}{2} \begin{pmatrix} 1 & e^{iE_j\tau} \\ e^{-iE_j\tau} & 1 \end{pmatrix}. \quad (\text{C10})$$

2. Entangled-ancillas protocol

Our goal is to determine the purity of the ancilla. In general, there is the relation $\rho \text{ pure} \Leftrightarrow \text{Tr}[\rho^2] = \lambda_1^2 + \lambda_2^2$ for density matrices, with λ_1 and λ_2 the eigenvalues of ρ . We write the density matrix and its square as

$$\rho_{\text{ancilla}} = \begin{pmatrix} a & b \\ c & d \end{pmatrix} \quad \text{and} \quad \rho_{\text{ancilla}}^2 = \begin{pmatrix} a^2 + bc & \cdot \\ \cdot & bc + d^2 \end{pmatrix} \quad (\text{C11})$$

where matrix elements irrelevant for our protocol are denoted with a dot. With the Bell state

$$|\Phi^-\rangle = \frac{1}{\sqrt{2}} (|00\rangle - |11\rangle) \quad (\text{C12})$$

we construct the Bell measurement operator

$$|\Phi^-\rangle \langle \Phi^-| = \frac{1}{2} \begin{pmatrix} 1 & 0 & 0 & -1 \\ 0 & 0 & 0 & 0 \\ 0 & 0 & 0 & 0 \\ -1 & 0 & 0 & 1 \end{pmatrix}. \quad (\text{C13})$$

The diagonal matrix elements of ρ_{ancilla}^2 may then be attained by considering a composite system where the second system with controlled backwards time evolution (implementable by changing the sign of H). Then, the density

matrix of the ancilla of the second system effectively corresponds to the transpose of the density matrix of the first ancilla $\rho_{\text{ancilla}2} = \rho_{\text{ancilla}1}^T$. The composite system then gives

$$\rho_{\text{ancilla}1} \otimes \rho_{\text{ancilla}2} = \rho_{\text{ancilla}1} \otimes \rho_{\text{ancilla}1}^T = \begin{pmatrix} a^2 & \cdot & \cdot & bc \\ \cdot & \cdot & \cdot & \cdot \\ \cdot & \cdot & \cdot & \cdot \\ bc & \cdot & \cdot & d^2 \end{pmatrix} = \frac{1}{4} \begin{pmatrix} 1 & \cdot & \cdot & |\alpha|^2 \\ \cdot & \cdot & \cdot & \cdot \\ \cdot & \cdot & \cdot & \cdot \\ |\alpha|^2 & \cdot & \cdot & 1 \end{pmatrix}. \quad (\text{C14})$$

If $|\psi\rangle$ is in an eigenstate, the density matrix of the ancilla ρ_{ancilla} is pure and the expectation of the $|\Phi^-\rangle$ measurement is

$$\langle \rho_{\text{ancilla}1} \otimes \rho_{\text{ancilla}2} \rangle_{|\Phi^-\rangle} = \frac{1}{4} (1 - |\alpha|^2) = 0, \quad (\text{C15})$$

3. Choosing suitable time values in the ancilla protocol

We have argued that a measure for the eigenstate closeness is given by

$$\langle \psi | \psi_{\text{evo}} \rangle = \langle \sigma_x - i\sigma_y \rangle_{\text{ancilla}} = \sum_j |\psi_j|^2 e^{-iE_j\tau} =: \alpha. \quad (\text{C16})$$

using the one-ancilla protocol. For suitable τ , $|\psi_{\text{evo}}\rangle$ is an eigenstate of the fixed Hamiltonian H only if $|\alpha| = 1$. The time τ needs to be chosen so that the complex summands of α with non-vanishing amplitude do not have approximately equal phases. In this unlikely case of matching phases, we would see constructive interference so that $\alpha = 1$ could be true even if $|\psi_{\text{evo}}\rangle$ is not an eigenstate. Visualizing the summands of α on a complex plane (Fig. 18), this becomes rather intuitive. The choice for τ is related to the spectrum of H . It is reasonable to assume and confirmed in our simulations that a quantum state in our algorithm has the largest overlap with the ground state. As transitions to high energy excited states are extremely rare, for this argument we assume that the overlap with the first excited state was the only other non-vanishing overlap. Then, we simply have

$$\alpha = |\psi_0|^2 e^{-iE_0\tau} + |\psi_1|^2 e^{-iE_1\tau}. \quad (\text{C17})$$

In the case of destructive interference

$$|\alpha| = \min_{\tau} |\alpha(\tau)| \quad (\text{C18})$$

which corresponds to

$$e^{-iE_0\tau} + e^{-iE_1\tau} \stackrel{!}{=} 0 \Leftrightarrow \tau(E_1 - E_0) = \pi(2k + 1) \quad (\text{C19})$$

$$\Leftrightarrow \tau = \frac{\pi}{\Delta}(2k + 1) \quad (\text{C20})$$

with $k \in \mathbb{Z}$ and $\Delta = E_1 - E_0$. An arbitrary τ would correspond to choosing an $l \in \mathbb{Z}$ in $\tau = \pi l / \Delta$ at random. For $l \gg 1$, the probability of choosing an odd value of l is approximately 1/2. Therefore, by testing several random values of $\tau \in O(\Delta^{-1})$ it is possible to deduce information about the system whether it is in a mixed state or an eigenstate with high confidence.

4. Bound for the single-ancilla protocol

We extend the discussion about suitable values of τ . As argued above, an answer is generally dependent on the spectral properties of H , which are not available a priori.

We shall provide a bound for the single ancilla method without any knowledge about the spectrum of H or the populations of the different eigenstates. A byeffect of this generality is that the bound is not tight. This is because in a realistic setting of a (quasi-)adiabatic evolution, the eigenstate populations of higher excites are expected to be very small.

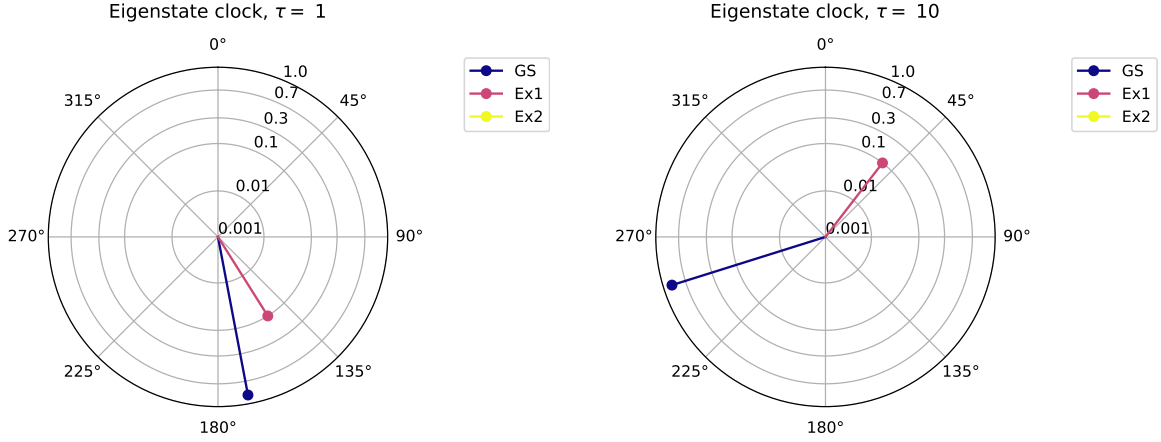


FIG. 18. Eigenstate clocks for two values of τ . For $\tau=1$ the summand corresponding to the ground state and the summand corresponding to the first excited state lie quite closely together in phase which leads to problematic constructive interference. However, as the pointers rotate with their respective eigenenergy for changing τ , they are well-separated for $\tau = 10$. Then, we find destructive interference in the summation which is necessary for the explanatory power of the protocol. Note that in this instance, the summands corresponding to higher excited eigenstates are very small and not visible.

We consider the expectation value [58] of $\alpha(\tau)$

$$\mathbb{E}_{\tau \sim \text{unif. dist. in } [0, K]}(|\alpha(\tau)|^2) = \frac{1}{K} \int_0^K |\alpha(\tau)|^2 d\tau \quad (\text{C21})$$

$$= \frac{1}{K} \int_0^K \sum_{i,j} |\psi_i|^2 |\psi_j|^2 e^{-iE_i \tau} e^{-iE_j \tau} d\tau \quad (\text{C22})$$

$$= \sum_{i,j} |\psi_i|^2 |\psi_j|^2 \text{sinc}((E_i - E_j)K). \quad (\text{C23})$$

In the limit of large K , we obtain

$$\lim_{K \rightarrow \infty} \mathbb{E}_{\tau \sim \text{unif. dist. in } [0, K]}(|\alpha(\tau)|^2) = \sum_i |\psi_i|^4 =: E^2 \quad (\text{C24})$$

where the spectral dependence has entirely averaged out. Such an E^2 corresponds to what one would observe in the laboratory. We note that $|\psi_0|^2$ was the ground state overlap of $|\psi\rangle$. As $|\psi\rangle$ is normalized, we can write

$$|\psi_i|^2 \leq 1 - |\psi_0|^2 \quad \forall i > 0, \quad (\text{C25})$$

i.e. for all i which do not correspond to the ground state. Then, multiplying with $|\psi_i|_{i>0}^2$ yields

$$|\psi_i|^4 \leq (1 - |\psi_0|^2) |\psi_i|^2 \quad \forall i > 0. \quad (\text{C26})$$

As the latter inequality holds for all $i > 0$, we obtain

$$\sum_{i=1} |\psi_i|^4 \leq (1 - |\psi_0|^2) \sum_{i=1} |\psi_i|^2 = (1 - |\psi_0|^2)^2. \quad (\text{C27})$$

For the expectation value E^2 we can now write down the inequality

$$E^2 = |\psi_0|^4 + \sum_{i=1} |\psi_i|^4 \leq |\psi_0|^4 + (1 - |\psi_0|^2)^2. \quad (\text{C28})$$

Solving for $|\psi_0|^2$, we obtain

$$|\psi_0|^2 \geq \frac{1}{2} + \frac{1}{2} \sqrt{2E^2 - 1}, \quad \text{or} \quad |\psi_0|^2 \leq \frac{1}{2} - \frac{1}{2} \sqrt{2E^2 - 1}. \quad (\text{C29})$$

So far we have not assumed anything about the populations. Letting the ground state population $|\psi_0|^2$ be the largest of the eigenstate populations, we have

$$|\psi_0|^2 \geq \frac{1}{2} + \frac{1}{2} \sqrt{2E^2 - 1} \quad (\text{C30})$$

as a lower bound for $|\psi_0|^2$ for $E^2 \geq 1/2$. Also, (Eqn. C29) implies that in this case the smaller ground state populations are therefore upper bounded as

$$|\psi_i|^2 \leq \frac{1}{2} - \frac{1}{2} \sqrt{2E^2 - 1} \quad \forall i > 0. \quad (\text{C31})$$

For $E^2 < 1/2$, no non-trivial bound for $|\psi_0|^2$ (apart from $|\psi_0|^2 \in [0, 1]$) can be given in the limit of very large K (with this approach).

Appendix D: Simulating the adiabatic evolution with matrix product states

1. Tensor network techniques

In order to describe a general N -qubit quantum state with d spin degrees of freedom, there are d^N coefficients c_{i_1, i_2, \dots, i_N} in

$$|\psi\rangle = \sum_{0 \leq i_1, i_2, \dots, i_N < d} c_{i_1, i_2, \dots, i_N} |i_1, i_2, \dots, i_N\rangle \quad (\text{D1})$$

that we need to account for. The $|i_k\rangle_{i=1}^d$ are forming an orthonormal basis of local Hilbert space (for $1 \leq k < N$). However, and to our great benefit, ground states of gaped local one-dimensional Hamiltonians obey an area law regarding their entanglement entropy [59]. In fact, area law states occupy an exponentially small corner of the many-body Hilbert space only, which makes a more economical description of the quantum state possible. If we consider the coefficients c_{i_1, i_2, \dots, i_N} being a very large tensor which can be decomposed into a chain of tensors of order 3, we obtain an alternative approach. We describe the quantum state by a matrix product state (MPS) ansatz for open boundary conditions by

$$|\psi_{\text{MPS}}\rangle = \sum_{0 \leq i_1, i_2, \dots, i_N < d} B_1^{i_1} B_2^{i_2} \dots B_N^{i_N} |i_1, i_2, \dots, i_N\rangle. \quad (\text{D2})$$

The complex matrices $B_k^{i_k}$ are $(D \times D)$ -dimensional with the exception of the boundary tensors which are vectors. D is the dimension of the virtual bonds in the MPS representation, limiting the amount of entanglement that can be represented by the MPS ansatz. Describing the state as a matrix product state only requires ND^2d parameters which is clearly preferable if a moderate virtual bond dimension D suffices. Therefore, MPS methods are an extremely successful ansatz to describe such quantum states obeying the area law such as aforementioned ground states [60]. In general, MPS are not well-suited to simulate the dynamics of a quantum system, due to the increase of entanglement in the system. However, in our algorithm which describes a (quasi-)adiabatic dynamic, the quantum states are very close to the ground state of the system. This making MPS a perfect candidate for classically simulating quantum adiabatic algorithms.

For the simulation of time evolution we employ the time-evolving block decimation algorithm (TEBD) [61] which is the computationally cheapest method of several time-evolution methods for tensor networks and it is also well-suited for Hamiltonians with local interactions. This being said, other powerful time-evolution methods have been developed in recent years, such as MPO W^{I,II}, TDVP and the global Krylov method [62].

An appealing property of the ZZXZ model is the suppressed the light cone spreading due to real time confinement [63]. This leads to a very slow increase in entanglement when time evolving the system, making this model a good candidate for simulations with MPS. The maximum bond dimension of the MPS could be kept at modest values while maintaining very good accuracy in the MPS representation.

2. Simulating noisy quantum circuits

In order to simulate noisy quantum circuits, two main approaches are feasible. A noisy quantum channel can be represented by working with density matrices instead of quantum states. This is because an MPS cannot represent

a mixed state. By considering Matrix Product Density Operators instead of MPS, such noisy quantum channels can be efficiently dealt with. We have chosen the second approach where noisy circuits are simulated through statistically averaging over an ensemble of MPS

$$\rho \rightarrow \rho_{\text{noisy}} = \frac{1}{n} \sum_{k=1}^n \underbrace{\mathcal{N}_k |\tilde{\psi}_k\rangle \langle \tilde{\psi}_k|}_{|\tilde{\psi}_k\rangle} \mathcal{N}_k^\dagger \quad (\text{D3})$$

with the noise tensors \mathcal{N} being unitary matrices. Each of the MPS $|\tilde{\psi}_k\rangle$ will be different due to the probabilistic nature of noise. In the limit of a large MPS sample size n , both approaches will yield the same results.

A discrete noise model is considered, where p is the noise strength and probability that a noise event occurs. Such a noise event can be either a bit flip (σ_x), a phase flip (σ_z) or a combination of both. The noise channel for discrete noise is

$$\rho \rightarrow \mathcal{N} \rho \mathcal{N}^\dagger = (1-p)\rho + \frac{p}{3}(\sigma_x \rho \sigma_x + \sigma_y \rho \sigma_y + \sigma_z \rho \sigma_z). \quad (\text{D4})$$

The distinct noise tensors $\{\mathcal{N}_i\}$ are contracted with respective tensors $\{B_i\}$ for $i \in \{1, \dots, N\}$ before the first and after every N -site unitary (Fig. 19). As an example, in the discrete noise model with noise strength of $p = 10^{-4}$,

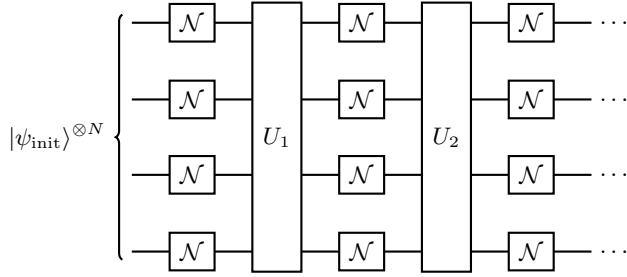


FIG. 19. Quantum circuit including the noise tensors \mathcal{N} which are all distinct from each other. Before and every N -site unitary, a noise event \mathcal{N} is applied to the respective tensor B_i .

$N = 100$ qubits, a time evolution for total time $T = 5$ and 16 discrete steps per time unit, we expect on average $10^{-4} \cdot 100 \cdot (1+5) \cdot 16 = 0.96 \approx 1$ noise event in the entire quantum circuit.

Appendix E: Plots on the number of measurements and noise

We include plots showing the number of ground state overlaps for an instance of the black box algorithm for $N = 100$ and five chunks. Also, we present an estimate of the number of measurements needed using the Chebyshev-Hoeffding inequality (Fig. 21). For a discussion of the inherent robustness of adiabatic algorithm, we show the energy density of states for $N = 12$ for the ZZXZ model (Fig. 22a) and an analysis of the relative energy error due to a noisy gate at different positions in the adiabatic evolution (Fig. 22b).

Appendix F: Bayesian inference in hypothesis testing

We give a brief summary on how to use Bayesian inference in order to do highly efficient hypothesis testing using our entangled-ancillas protocol (Sec. IV B) to decide whether the ground state overlap is larger than a given threshold value. In an experimental setup, we would like to only obtain as few samples as needed. Therefore, after each measurement, we would like to make use of a stopping criterion to decide whether we need to continue sampling or are able to terminate. Unfortunately, stopping rules are quite cumbersome to deal with in a frequentist approach. And fortunately, Bayesian inference turns out to be a most convenient tool.

The measurement outcomes of a quantum expectation value such as the ground state overlap with our protocol are assumed to behave as an independent and identically distributed (i.i.d.) random Bernoulli variable. The total measurement data is $X = \{x_1, \dots, x_N\}$ with a Beta prior $\theta = \text{Beta}(a_i, b_i)$. The prior prevents overfitting for few data points. The Beta distribution is normalized and given as

$$\text{Beta}(\mu|a, b) = \frac{\Gamma(a+b)}{\Gamma(a)\Gamma(b)} \mu^{a-1} (1-\mu)^{b-1} \quad (\text{F1})$$

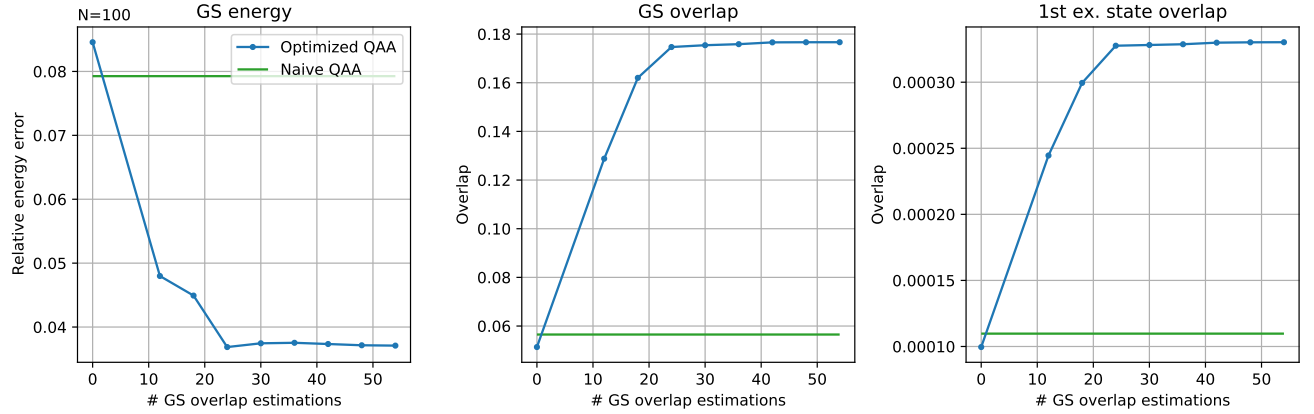


FIG. 20. Number of iterations needed for this instance. The optimizer algorithm is L-BFGS-M without any further adjustments. Very good results are already obtained after three iterations and less than 25 ground state overlap evaluations. The data corresponds to the first eight iterations of an instance of the black box optimizer with five chunks for fixed total time $T = 1$ and $N = 100$.

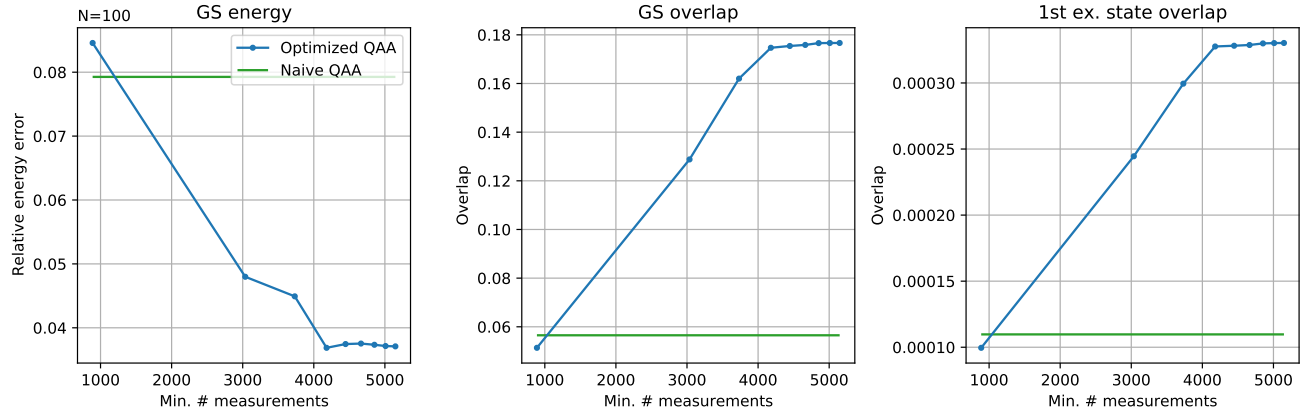


FIG. 21. Number of measurement in the instance. The number of measurements have been obtained using the Chernoff-Hoeffding inequality and the assumptions put down in the main text. Already for few thousand total measurement, the end result of the adiabatic evolution is significantly improved. The data corresponds to the first eight iterations of an instance of the black box optimizer with five chunks for fixed total time $T = 1$ and $N = 100$.

with

$$\Gamma(x) = \int_0^\infty \mu^{x-1} e^{-\mu} d\mu. \quad (\text{F2})$$

The mean and the variance of the Beta distribution are

$$\mathbb{E}[X] = \frac{a}{a+b}, \quad (\text{F3})$$

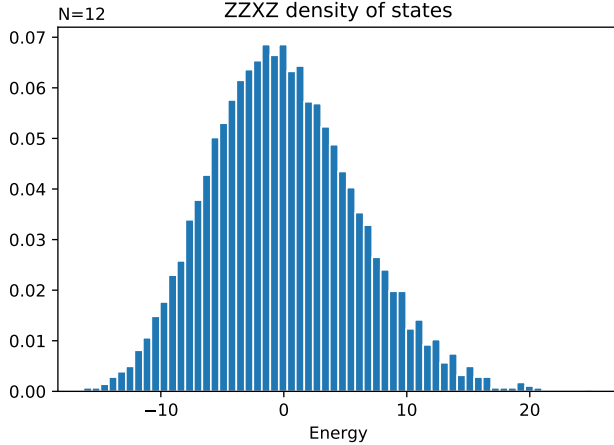
$$\text{var}[X] = \frac{ab}{(a+b)^2(a+b+1)}. \quad (\text{F4})$$

The Beta distribution is the conjugated prior for the Bernoulli distribution, implying that the posterior after one measurement is again a Beta distribution with new parameters [64]:

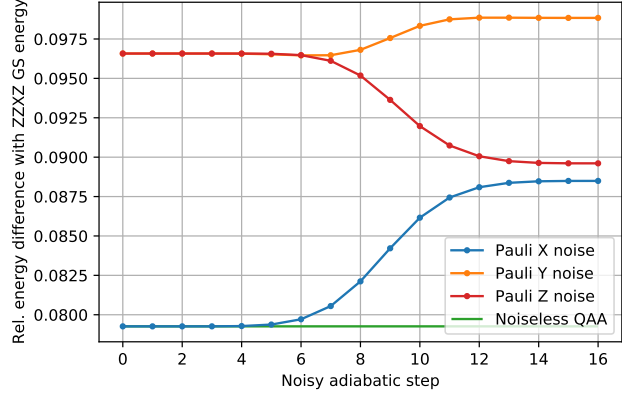
$$p(\theta|X) \propto \prod_{n=1}^N p(x_n|\theta)p(\theta) \quad (\text{F5})$$

$$= \prod_{n=1}^N \theta^{x_n} (1-\theta)^{1-x_n} \frac{1}{\text{Beta}(a,b)} \theta^{a-1} (1-\theta)^{b-1} \quad (\text{F6})$$

$$\propto \theta^{\sum_{i=1}^N x_i + a - 1} (1-\theta)^{N - \sum_{i=1}^N x_i + b - 1}. \quad (\text{F7})$$



(a) The energy density of states of the ZZXZ model for $N = 12$. Low energy spectral lines are rare for physical instances.



(b) Relative energy difference with ZZXZ ground state obtained with DMRG for adiabatic ground state preparation. The total time is fixed to $T = 1$ corresponding to 16 discrete adiabatic steps. Pauli noise is applied either before the first unitary (step 0) or after each unitary to the center qubit of

the spin chain. We observe that there is no qualitative difference at which position in the adiabatic path noise occurs.

Note that for a σ^x noise gate, there is no difference in the energy at the beginning of the adiabatic path because the initial Hamiltonian H_0 commutes with σ^x .

FIG. 22. Further plots on the robustness of the adiabatic evolution.

When sampling in the experiment, our posterior becomes the prior for the next measurement until our stopping criterion is fulfilled. We merely need to keep track of the 0's and 1's or spin-ups and spin-downs that are measured.

$$p(\theta|X) = \text{Beta}(a_N, b_N), \quad (\text{F8})$$

$$a_N = \sum_{i=1}^N x_i + a, \quad (\text{F9})$$

$$b_N = N - \sum_{i=1}^N x_i + b. \quad (\text{F10})$$

If we are expecting mostly zeros when close to the ground state, we might initialize our prior with $a = 10$ and $b = 2$. If the algorithm asks for a ground state overlap greater than H_0 (Zero hypothesis: $|\langle \psi | \psi_{\text{evo}} \rangle| > H_0$), samples are gathered until a stopping criterion is met and H_0 is either accepted or rejected. A decision upon the hypothesis is hard when H_0 is very close to the mean as many samples will be necessary to distinguish them. Setting up an interval $[H_0 - \epsilon, H_0 + \epsilon]$ where a decision cannot be made overcomes this problem. Then, H_0 can be updated to a different value and the sampling is restarted. The following outcomes of hypothesis testing are possible:

Algorithm 1: Decision algorithm for hypothesis testing

```

Set  $\alpha$ -threshold
for  $i$  to Maximum number of samples do
  Take sample number  $i$ 
  Update left and right  $\alpha$ -error
  if Left  $\alpha$ -error  $< \alpha$ -threshold then
    | Accept hypothesis
  else if Right  $\alpha$ -error  $< \alpha$ -threshold then
    | Reject hypothesis
end
if Hypothesis can be neither accepted nor rejected then
  | Update  $\alpha$ -threshold and repeat

```

Identifying a 0-measurement (perfect ground state overlap) with increasing a by 1 and a 1-measurement with increasing b by 1, the a_N and b_N contain the sampling data after N samples. When close to a ground state, we expect mainly 0's to be counted and a distribution strongly biased towards $p = 1$. A suitable stopping criterion might be an alpha

error probability of under 5%. A sample case is shown in (Fig. 23).

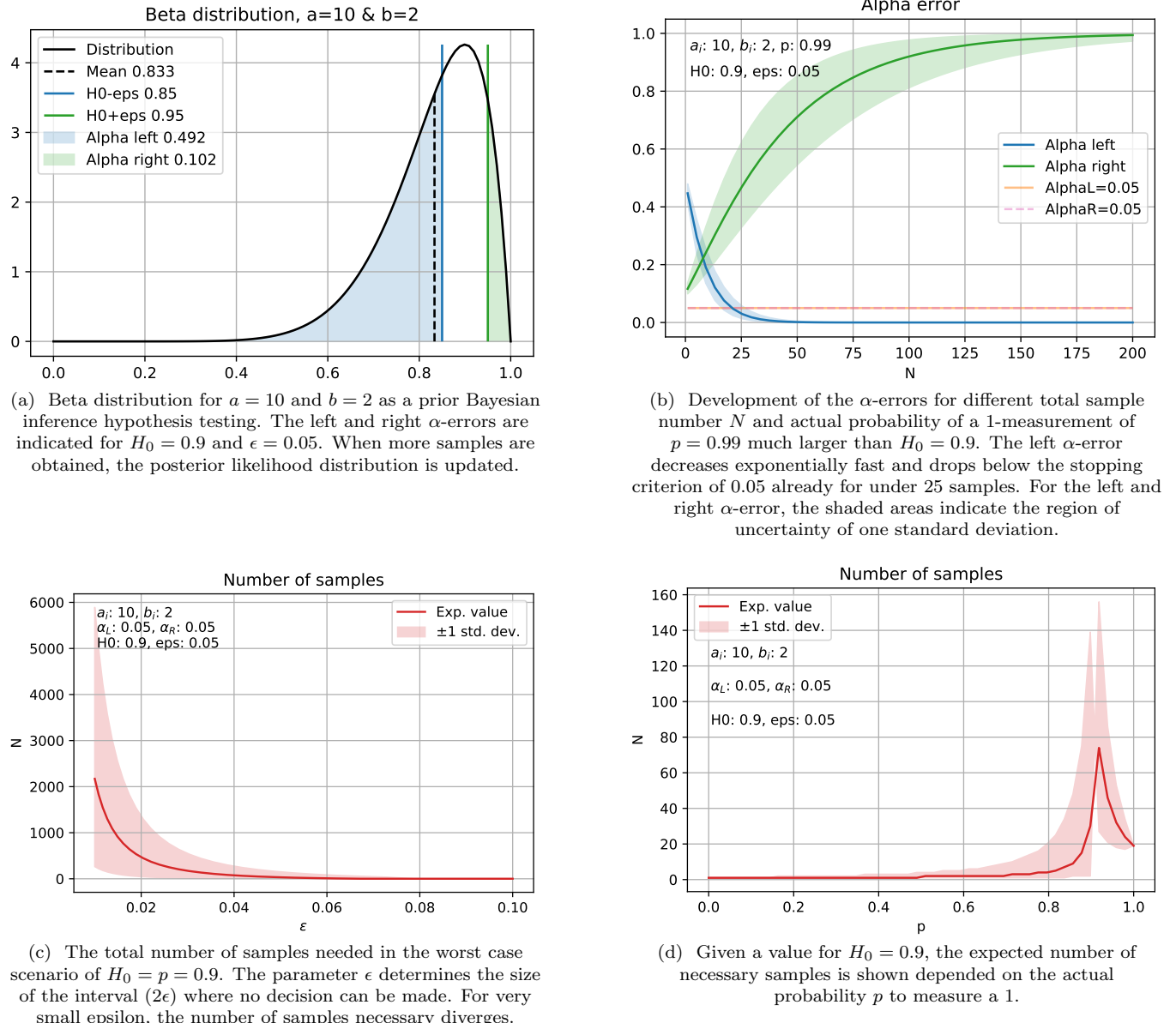


FIG. 23. Example for Bayesian hypothesis testing.

[1] J. Preskill, Quantum computing in the NISQ era and beyond, *Quantum* **2**, 79 (2018).

[2] F. Arute, K. Arya, R. Babbush, D. Bacon, J. C. Bardin, R. Barends, R. Biswas, S. Boixo, F. G. Brandao, D. A. Buell, *et al.*, Quantum supremacy using a programmable superconducting processor, *Nature* **574**, 505 (2019).

[3] H.-S. Zhong, H. Wang, Y.-H. Deng, M.-C. Chen, L.-C. Peng, Y.-H. Luo, J. Qin, D. Wu, X. Ding, Y. Hu, *et al.*, Quantum computational advantage using photons, *Science* **370**, 1460 (2020).

[4] G. Wordin, Quantum information processing with superconducting circuits: a review, *Reports on Progress in Physics* **80**, 106001 (2017).

[5] J. I. Cirac and P. Zoller, Goals and opportunities in quantum simulation, *Nature Physics* **8**, 264 (2012).

[6] C. Gross and I. Bloch, Quantum simulations with ultracold atoms in optical lattices, *Science* **357**, 995 (2017).

[7] J. Kempe, A. Kitaev, and O. Regev, The complexity of the local Hamiltonian problem, *SIAM Journal on Computing* **35**, 1070 (2006).

[8] E. Farhi, J. Goldstone, S. Gutmann, and M. Sipser, Quantum computation by adiabatic evolution, *arXiv preprint quant-ph/0001106* (2000).

[9] A. Messiah, *Quantum mechanics: Volume II* (North-Holland Publishing Company Amsterdam, 1962).

[10] M. H. Amin, Consistency of the adiabatic theorem, *Physical review letters* **102**, 220401 (2009).

[11] S. Jansen, M.-B. Ruskai, and R. Seiler, Bounds for the adiabatic approximation with applications to quantum computation, *Journal of Mathematical Physics* **48**, 102111 (2007).

[12] A. Elgart and G. A. Hagedorn, A note on the switching adiabatic theorem, *Journal of Mathematical Physics* **53**, 102202 (2012).

[13] E. Farhi, J. Goldstone, and S. Gutmann, A quantum approximate optimization algorithm, *arXiv preprint arXiv:1411.4028* (2014).

[14] S. Wang, E. Fontana, M. Cerezo, K. Sharma, A. Sone, L. Cincio, and P. J. Coles, Noise-induced barren plateaus in variational quantum algorithms, *arXiv preprint arXiv:2007.14384* (2020).

[15] D. S. Franca and R. Garcia-Patron, Limitations of optimization algorithms on noisy quantum devices, *arXiv preprint arXiv:2009.05532* (2020).

[16] M. Cerezo, A. Arrasmith, R. Babbush, S. C. Benjamin, S. Endo, K. Fujii, J. R. McClean, K. Mitarai, X. Yuan, L. Cincio, *et al.*, Variational quantum algorithms, *arXiv preprint arXiv:2012.09265* (2020).

[17] L. Bittel and M. Kliesch, Training variational quantum algorithms is NP-hard—even for logarithmically many qubits and free fermionic systems, *arXiv preprint arXiv:2101.07267* (2021).

[18] M. A. Nielsen and I. L. Chuang, *Quantum Computation and Quantum Information (10th Anniversary edition)* (Cambridge University Press, 2016).

[19] Y. Chen and T.-C. Wei, Quantum algorithm for spectral projection by measuring an ancilla iteratively, *Physical Review A* **101**, 032339 (2020).

[20] The state $|+\rangle$ is an eigenvector of the Pauli matrix σ^x and defined as $|+\rangle = (|0\rangle + |1\rangle)/\sqrt{2}$ where $|0\rangle$ and $|1\rangle$ are the computational basis states.

[21] R. Santagati, J. Wang, A. A. Gentile, S. Paesani, N. Wiebe, J. R. McClean, S. Morley-Short, P. J. Shadbolt, D. Bonneau, J. W. Silverstone, *et al.*, Witnessing eigenstates for quantum simulation of Hamiltonian spectra, *Science advances* **4**, eaap9646 (2018).

[22] T. E. O'Brien, S. Polla, N. C. Rubin, W. J. Huggins, S. McArdle, S. Boixo, J. R. McClean, and R. Babbush, Error mitigation via verified phase estimation, *arXiv preprint arXiv:2010.02538* (2020).

[23] P. Magnard, S. Storz, P. Kurpiers, J. Schär, F. Marxer, J. Lütolf, T. Walter, J.-C. Besse, M. Gabureac, K. Reuer, *et al.*, Microwave quantum link between superconducting circuits housed in spatially separated cryogenic systems, *Physical Review Letters* **125**, 260502 (2020).

[24] K. Boothby, P. Bunyk, J. Raymond, and A. Roy, Next-generation topology of D-Wave quantum processors, *arXiv preprint arXiv:2003.00133* (2020).

[25] R. H. Byrd, P. Lu, J. Nocedal, and C. Zhu, A limited memory algorithm for bound constrained optimization, *SIAM Journal on scientific computing* **16**, 1190 (1995).

[26] J. A. Nelder and R. Mead, A simplex method for function minimization, *The Computer Journal* **7**, 308 (1965).

[27] I. Cirac, D. Perez-Garcia, N. Schuch, and F. Verstraete, Matrix product states and projected entangled pair states: Concepts, symmetries, and theorems, *arXiv preprint arXiv:2011.12127* (2020).

[28] The Pauli matrices are defined as $\sigma_x = \begin{pmatrix} 0 & 1 \\ 1 & 0 \end{pmatrix}$, $\sigma_y = \begin{pmatrix} 0 & -i \\ i & 0 \end{pmatrix}$ and $\sigma_z = \begin{pmatrix} 1 & 0 \\ 0 & -1 \end{pmatrix}$.

[29] A. Ovchinnikov, D. Dmitriev, V. Y. Krivnov, and V. Cheranovskii, Antiferromagnetic Ising chain in a mixed transverse and longitudinal magnetic field, *Physical review B* **68**, 214406 (2003).

[30] M. Novotny and D. Landau, Zero temperature phase diagram for the d=1 quantum Ising antiferromagnet, *Journal of Magnetism and Magnetic Materials* **54**, 685 (1986).

[31] A. Benseñy and K. Mølmer, All's well that ends well: the unexpectedly good performance of adiabatic passage, *arXiv preprint arXiv:2010.05093* (2020).

[32] L. Zhou, S.-T. Wang, S. Choi, H. Pichler, and M. D. Lukin, Quantum approximate optimization algorithm: Performance, mechanism, and implementation on near-term devices, *Physical Review X* **10**, 021067 (2020).

[33] W. Hoeffding, Probability inequalities for sums of bounded random variables, in *The Collected Works of Wassily Hoeffding* (Springer, 1994) pp. 409–426.

[34] Y. Zhou, E. M. Stoudenmire, and X. Waintal, What limits the simulation of quantum computers?, *Physical Review X* **10**, 041038 (2020).

[35] A. M. Childs, E. Farhi, and J. Preskill, Robustness of adiabatic quantum computation, *Physical Review A* **65**, 012322 (2001).

[36] S. Lu, M. C. Bañuls, and J. I. Cirac, Algorithms for quantum simulation at finite energies, *arXiv preprint arXiv:2006.03032* (2020).

[37] E. Urban, T. A. Johnson, T. Henage, L. Isenhower, D. Yavuz, T. Walker, and M. Saffman, Observation of Rydberg blockade between two atoms, *Nature Physics* **5**, 110 (2009).

[38] T. Albash and D. A. Lidar, Adiabatic quantum computation, *Reviews of Modern Physics* **90**, 015002 (2018).

[39] J. Roland and N. J. Cerf, Quantum search by local adiabatic evolution, *Physical Review A* **65**, 042308 (2002).

[40] A. Rezakhani, W.-J. Kuo, A. Hamma, D. Lidar, and P. Zanardi, Quantum adiabatic brachistochrone, *Physical review letters* **103**, 080502 (2009).

[41] J. Lin, Z. Y. Lai, and X. Li, Quantum adiabatic algorithm design using reinforcement learning, *Physical Review A* **101**, 052327 (2020).

[42] X. Bonet-Monroig, R. Babbush, and T. E. O'Brien, Nearly optimal measurement scheduling for partial tomography of quantum states, *Physical Review X* **10**, 031064 (2020).

[43] B. Koczor, Exponential error suppression for near-term quantum devices, *arXiv preprint arXiv:2011.05942* (2020).

[44] W. J. Huggins, S. McArdle, T. E. O'Brien, J. Lee, N. C. Rubin, S. Boixo, K. B. Whaley, R. Babbush, and J. R. McClean, Virtual distillation for quantum error mitigation, *arXiv preprint arXiv:2011.07064* (2020).

[45] S. Boixo, E. Knill, and R. D. Somma, Eigenpath traversal by phase randomization, *Quantum Inf. Comput.* **9**, 833 (2009).

[46] M. Banuls, R. Orús, J. Latorre, A. Pérez, and P. Ruiz-Femenia, Simulation of many-qubit quantum computation with matrix product states, *Physical Review A* **73**, 022344 (2006).

[47] N. Hatano and M. Suzuki, Finding exponential product formulas of higher orders, in *Quantum annealing and other optimization methods* (Springer, 2005) pp. 37–68.

[48] U. Schollwöck, The density-matrix renormalization group in the age of matrix product states, *Annals of physics* **326**, 96 (2011).

[49] M. C. Bañuls, K. Cichy, J. I. Cirac, and K. Jansen, The mass spectrum of the Schwinger model with matrix product states, *Journal of High Energy Physics* **2013**, 158 (2013).

[50] J. Haensch and F. Pollmann, Efficient numerical simulations with Tensor Networks: Tensor Network Python (TeNPy), *SciPost Phys. Lect. Notes* , 5 (2018).

[51] D. Chruscinski and A. Jamiolkowski, *Geometric phases in classical and quantum mechanics*, Vol. 36 (Springer Science & Business Media, 2012).

[52] M. V. Berry, Quantal phase factors accompanying adiabatic changes, *Proceedings of the Royal Society of London. A. Mathematical and Physical Sciences* **392**, 45 (1984).

[53] A. Kay, Tutorial on the quantikz package, *arXiv preprint arXiv:1809.03842* (2018).

[54] For an initial Hamiltonian $H_0 = \sum_{j=1}^N \sigma_j^x$, the state $|+\rangle^{\otimes N}$ is usually chosen to be the initial state. However, the ground state of H_0 is $|-\rangle^{\otimes N}$ and it would correspond to the initial state of an adiabatic quantum algorithm.

[55] L. D. Landau, Zur Theorie der Energieübertragung II, *Z. Sowjetunion* **2**, 46 (1932).

[56] C. Zener, Non-adiabatic crossing of energy levels, *Proceedings of the Royal Society of London. Series A, Containing Papers of a Mathematical and Physical Character* **137**, 696 (1932).

[57] C. De Grandi and A. Polkovnikov, Adiabatic perturbation theory: From Landau–Zener problem to quenching through a quantum critical point, in *Quantum Quenching, Annealing and Computation* (Springer, 2010) pp. 75–114.

[58] In writing the expectation value, we make use of the (unnormalized) sinc function which is defined as $\text{sinc}(x) := \sin(x)/x$.

[59] M. B. Hastings, An area law for one-dimensional quantum systems, *Journal of Statistical Mechanics: Theory and Experiment* **2007**, P08024 (2007).

[60] F. Verstraete and J. I. Cirac, Matrix product states represent ground states faithfully, *Physical Review B* **73**, 094423 (2006).

[61] G. Vidal, Efficient simulation of one-dimensional quantum many-body systems, *Physical review letters* **93**, 040502 (2004).

[62] S. Paeckel, T. Köhler, A. Swoboda, S. R. Manmana, U. Schollwöck, and C. Hubig, Time-evolution methods for matrix-product states, *Annals of Physics* **411**, 167998 (2019).

[63] M. Kormos, M. Collura, G. Takács, and P. Calabrese, Real-time confinement following a quantum quench to a non-integrable model, *Nature Physics* **13**, 246 (2017).

[64] G. Gundersen, *Bayesian inference for Beta–Bernoulli models* (2020), accessed: 12 February 2021.

Numerical simulations	
Estimated project-related cluster kernel hours	245,000
Est. thermal design power per kernel [W]	6.25
Total energy consumption of simulations [kWh]	1,530
Est. specific emissions in Germany [kgCO ₂ eq/kWh]	0.5
Total CO ₂ eq emissions for numerical simulations [kg]	765
Transport	
No substantial project-related CO ₂ eq emissions for transport.	
Total	
CO ₂ eq emissions [kg]	765
<i>Emissions have been offset with atmosfair.de.</i>	

TABLE I. Table of project-related CO₂eq emissions. While some figures can only be estimated approximately, this information is intended to increase transparency about the climate impact of this project. Disclosing emissions of scientific research can help to raise awareness for the climate crisis. See also scientific-conduct.github.io.